Palaeometabolomes yield biological and ecological profiles at early human sites

Timothy G Bromage, Christiane C. Denys, Christopher Lawrence de Jesus, Hediye Erdjument-Bromage, Ottmar Kullmer, Oliver Sandrock, Friedemann Schrenk, Marc D Mckee, Natalie Reznikov, Gail M Ashley, et al.

Article

Palaeometabolomes yield biological and ecological profiles at early human sites

https://doi.org/10.1038/s41586-025-09843-w

Received: 5 August 2022

Accepted: 31 October 2025

Published online: 17 December 2025

Open access

Check for updates

Timothy G. Bromage[1,2,3]✉, Christiane Denys[4], Christopher Lawrence De Jesus[5], Hediye Erdjument-Bromage[5], Ottmar Kullmer[3,6], Oliver Sandrock[7], Friedemann Schrenk[3,6], Marc D. McKee[8,9], Natalie Reznikov[8,9,10], Gail M. Ashley[11], Bin Hu[1], Sher B. Poudel[12], Antoine Souron[13], Daniel J. Buss[8,9], Eran Ittah[10], Jülide Kubat[3], Sasan Rabieh[14], Shoshana Yakar[1] & Thomas A. Neubert[5]

The science of metabolic profiling exploits chemical compound byproducts of metabolism called metabolites[1] that explain internal biological functions, physiological health and disease, and provide evidence of external influences specific to an organism's habitat. Here we assess palaeometabolomes from fossilized mammalian hard tissues as a molecular ecological strategy to provide evidence of an ancient organism's relationship with its environment. From eastern, central and southern African Plio-Pleistocene localities of palaeoanthropological significance, we study six fossils from Olduvai Gorge, Tanzania, one from the Chiwondo Beds, Malawi, and one from Makapansgat, South Africa. We perform endogeneity assessments by analysing palaeometabolomes of palaeosols and the effects of owl digestion on rodent bones to enable prudent ecological inferences. Diagenesis is indicated by metabolites of collagenase-producing bacteria[2], whereas the preservation of peptides including those of collagen are identified by proteomics. Endogenous metabolites document biological functions and exogenous metabolites render environmental details including soil characteristics and woody cover, and enable annual minimum and maximum rainfall and temperature reconstructions at Olduvai Gorge, supporting the freshwater woodland and grasslands of Olduvai Gorge Bed I[3–5], and the dry woodlands and marsh of Olduvai Gorge Upper Bed II[6]. All sites denote wetter and/or warmer conditions than today. We infer that metabolites preserved in hard tissues derive from an extravasated vasculature serum filtrate that becomes entombed within developing mineralized matrices, and most probably survive palaeontological timeframes in the nanoscopic 'pool' of structural-bound water that occurs in hard tissue niches[7].

The metabolic rate of an organism is the sum of the energy necessary to acquire, convert and allocate energy to growth, reproduction and maintenance, which sets energetic limits on biological activities and establishes the pace and pattern of life[8–10]. The temperature- and mass-dependence of metabolic rate, from the smallest unicellular organisms to the largest plants and animals[9], enables one to reconstruct the metabolic rates of extinct organisms and retrodict fundamental large-scale features of their palaeoenvironments[11]. Otherwise, efforts to obtain knowledge of internal and external influences on fossil vertebrate metabolism have been limited to bone microanatomical correlates of thermophysiology[12] and palaeoenvironmental reconstructions, which typically depend on studies of stable isotopes, faunal composition and community ecology, dental wear analyses, and/or palynology or palaeovegetation in geological context[3,13,14].

Here we explore molecular ecological strategies for obtaining ultrafine-scale details of an ancient organism's metabolism that: (1) reflect its internal physiological responses to environmental conditions; and (2) reflect the diet that fuelled its metabolic rate. Metabolomic profiling of animals is typically performed on whole blood or its components, such as plasma, and on its transudates, such as urine and saliva[1]. However, we have learned that preservation niches that contain metabolites that were once in the free circulation exist within the mineralized tissue ultrastructure, being not too 'loose' (where they may be shielded) and not too 'tight' (where they may be permeable), as

[1]Department of Molecular Pathobiology, New York University College of Dentistry, New York, NY, USA. [2]Department of Anthropology, New York University, New York, NY, USA. [3]Senckenberg Research Institute and Natural History Museum, Frankfurt am Main, Germany. [4]Institute of Systematics and Evolution of Biodiversity, National Museum of Natural History, Paris, France. [5]Department of Neuroscience and Physiology and Neuroscience Institute, NYU Grossman School of Medicine, New York, NY, USA. [6]Institute of Ecology, Evolution and Diversity, Goethe University, Frankfurt am Main, Germany. [7]Earth and Life History, Hessisches Landesmuseum Darmstadt, Darmstadt, Germany. [8]Faculty of Dental Medicine and Oral Health Sciences, McGill University, Montreal, Quebec, Canada. [9]Department of Anatomy and Cell Biology, McGill University, Montreal, Quebec, Canada. [10]Department of Bioengineering, McGill University, Montreal, Quebec, Canada. [11]Department of Earth and Planetary Sciences, Rutgers, the State University of New Jersey, New Brunswick, NJ, USA. [12]Eurofins Lancaster Laboratories PSS, Lancaster, PA, USA. [13]Université de Bordeaux, CNRS, Ministère de la Culture, PACEA, UMR 5199, Pessac, France. [14]Department of Dental Hygiene and Dental Assisting, New York University College of Dentistry, New York, NY, USA. ✉e-mail: tim.bromage@nyu.edu

Table 1 | Fresh laboratory mouse bones and diets, fossils, and extant comparators for fossil taxa and palaeosols examined

Site category	Specimen code	Site or source	Taxon details
Comparative extant mouse			
Heterogeneous mouse and diet	2814–2818 and 2829–2833	The Jackson Laboratory	5F and 5M UM-HET3 mouse
Inbred mouse and diet	2092–2093, 2095–2098	The Jackson Laboratory	6F C57BL/6J mouse
Inbred mouse enzyme experiment	F/T3a, F/T3a (2 untreated) and F/T1-EZ, F/T2-Ez (2 treated)	The Jackson Laboratory	4F C57BL/6J mouse
Olduvai Gorge Bed I (1.7–1.8 Ma)			
Fossils	M-D	FLKN1 M3/*Bubo lacteus* pellet	*Mus* sp. or *Dendromus* sp.
	Sm	FLKN1/owl pellet	*Saccostomus* cf. *mearnsi*
	Gg	FLKN1 M1/*Bubo africanus* pellet	*Gerbilliscus gentryi*
	Gi	DK/probable *Bubo* sp. pellet	*Gerbilliscus* sp. indet.
	Xi	FLKN1 M3/*Bubo lacteus* pellet	*Xerus* cf. *inauris*
Olduvai Gorge Bed II (1.3 Ma)	von Koenigswald 1954	Olduvai	*Kolpochoerus majus*
Palaeosols for Bed I OG Samples	GA-01-08	Olduvai	Dryland soil carbonate
	GA-03-08	Olduvai	Dryland soil carbonate
	GA-39-16	Olduvai	Wetland soil carbonate
	GA-84-11	Olduvai	Wetland soil carbonate
	GA-94-11	Olduvai	Wetland soil carbonate
	GA-98-11	Olduvai	Wetland soil carbonate
Extant	MNHN CD	Olduvai *Bubo lacteus* owl pellet	*Mus* sp. or *Dendromus* sp.
	MNHN-ZM-MO 1991-817	Omo Valley live capture	*Saccostomus* cf. *mearnsi*
	MNHN-ZM-2024-4132	Olduvai *Bubo* sp. owl pellet	*Gerbilliscus* sp.
	MNHN-ZM-MO 2005-575	Olduvai live capture	*Xerus* sp.
Chiwondo Beds (2.4 Ma)			
Fossil	HCRP-RC-11 883	Chiwondo Beds	*Elephas recki shungurensis*
Palaeosol	HCRP-RC-11	Chiwondo Beds	
Extant	EE	Malawi	*Loxodonta africana*
Makapansgat (3 Ma)			
Fossil	TF12 Lime Dumps	Makapansgat	Bovidae
Palaeosols; grey breccia	TF12 Lime Dumps	Makapansgat	Sediment
Extant	EW	Malawi	*Kobus ellipsiprymnus*

we describe in the 'Analysis of bone mineral niches' section of the Methods, as well as potentially within the crystalline matrices of palaeosols. We posit that metabolites in hard tissue mineral niches are a serum transudate that has become entombed in the mineralizing extracellular matrix. Metabolites putatively survive in small compartments of interstitial water that are present in these hierarchically structured organic–inorganic interfaces[7].

"Palaeo-metabolomics" has been advanced to examine metabolite identities of scent from organic residues[15] and tobacco use as obtained from drilled bone samples[16] in the historic archaeological record. Here we provide genuine palaeometabolomes from the prehistoric fossil record using metabolomics as a systems biological approach and document that metabolites preserved in Plio-Pleistocene fossils may be used to study physiological health and disease of past life and research the palaeoecology.

The palaeometabolome recovered from a bone or tooth differs from the instantaneous metabolome of an organism obtained from biofluid, such as blood, urine or saliva. Instead, metabolites will have become stochastically trapped in mineral niches during the entire period of hard tissue formation. However, because size and shape changes remove bone (known as remodelling) formed during periods of early development[17], peak bone mass at skeletal maturity of any one bone will not encompass the entire period of its growth. Thus, by a rough approximation to periods of maturity, adult mouse cortical bone will harbour a metabolite accumulation of several months, bone of a ground squirrel will contain metabolites accumulated over less than one year, and so on for larger mammals, reaching several years if not decadal for a modern human, depending on the bone. Animals that secondarily remodel their cortical bone and trabecular bone surfaces potentially enable the recovery of metabolites for the remainder of their lifetime.

Samples analysed in this study are listed in Table 1. Fossil samples were from early human localities in eastern, central and southern Africa. Five fossil rodent bones derive from Bed I at Olduvai Gorge, Tanzania (from 1.8–1.7 million years ago (Ma)), and one suid fossil derives from Bed II (from 1.3 Ma) at this locality. We advance an ecogeographic perspective by analysing an elephantid dentine and cementum sample (from 2.4 Ma) from the Chiwondo Beds, Malawi, and a presumed bovid bone sample (from 3.0 Ma) from the site at Makapansgat, South Africa. In addition to the fossils, palaeosols from the localities and extant representatives of the fossil taxa have been analysed for endogeneity and quality control (a detailed list of all samples is presented in Supplementary Table 1.

We chose to particularly represent the Olduvai Gorge fossiliferous locality for two reasons: (1) the original semi-arid environmental reconstruction has recently been re-examined to include dense woodland and wetland[3], to which we predicted exogenous metabolites of the palaeometabolomes might correspond; and (2) fossil owl pellets at Olduvai Gorge contain identifiable rodent remains in abundance.

We focus on metabolites traceable to two major categories: (1) endogenous byproducts of metabolism that reflect internal metabolic processes, some of which present themselves in response to environmental factors, such as an infection or poor nutrition; and (2) exogenous

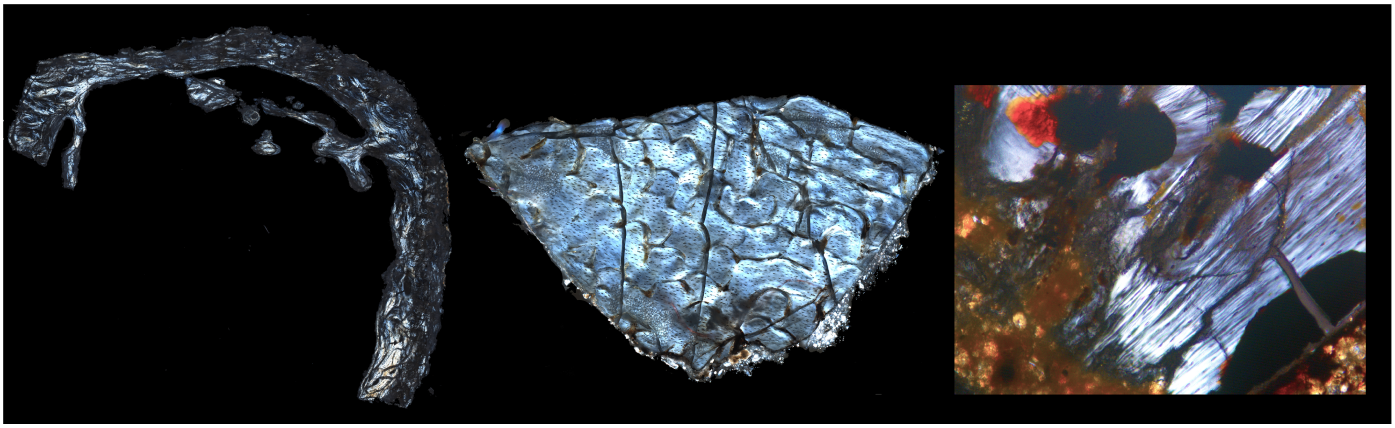

Fig. 1 | Representative images of fossil specimens. Images are of fossils from Olduvai Gorge (left; *Xerus* cf. *inauris* bone; field width (FW) = 4.434 mm), Chiwondo Beds (middle; *Elephas recki shungurensis* dentine; FW = 6.5 mm) and Makapansgat (right; Bovidae bone; FW = 80 µm). Brightness in the images is taken to be birefringence of collagen (the brown hue on the right is diagenetic alteration).

metabolites derived from organisms they consume. Because the tropics and subtropics have been the focus of intense drug and cosmetic discovery efforts for factors derived from medicinal plants[18,19], there is an increasing amount of plant metabolomics data available to draw on[20]. Recovering metabolites from these two categories enables us to address directly the questions of what metabolites are found in hard tissues that enable an interpretation of physiological signals and responses to the environment, and what metabolites derive from consumption patterns that fuelled their metabolisms.

We also performed metabolomics on fresh laboratory mouse bone samples—secondarily acquired from research investigations having no relationship to this study—and the diets of these mice to validate our retrieval and detection of metabolites. We also undertook an endogeneity assessment by performing metabolomics on palaeosols of the sites from which the fossils were excavated, because metabolites are present in soil that relate mainly to plant and microbial biological functions; palaeosol metabolites detected in common with fossil samples must putatively be removed from consideration of interpretations of exogenous metabolomes. Our assessment also includes an evaluation of the potential influence of the digestive system on the metabolomes obtained from the bones of rodents derived from regurgitated owl pellets.

Sample integrity

Prior to metabolite recovery, a portion of each fossil sample was subjected to histology and imaged by polarized light to illustrate putative collagen birefringence (Fig. 1). We present images for the five Olduvia Gorge rodent samples: specimen M-D (Extended Data Fig. 1), specimen Sm (Extended Data Fig. 2), specimen Gg (Extended Data Fig. 3), specimen Gi (Extended Data Fig. 4) and specimen Xi (Extended Data Fig. 5). Polarized light images are also presented for the Chiwondo Beds specimen HCRP-RC-11 883 (Supplementary Fig. 1) and the Makapansgat specimen TF12 Lime Dumps (Supplementary Fig. 2). Backscattered electron imaging in the scanning electron microscope (BSE-SEM) was also performed on the five Olduvai Gorge rodent specimens (Extended Data Figs. 6–10) and those of the Chiwondo Beds and Makapansgat specimens to confirm recognizable hard tissue microstructure (Supplementary Figs. 3 and 4).

To establish protein biomolecular integrity, proteomics analyses were performed on a representative of each Olduvai Gorge fossil rodent genus sampled (M-D, Sm, Gg and Xi), which revealed peptides related to collagen matrices (Supplementary Figs. 5 and 6), and other potentially exogenous peptides, including some from a parasitic infection (Supplementary Fig. 7).

Histology sections from the extant, fossil and palaeosol samples were also imaged by BSE-SEM for energy dispersive spectroscopy (EDS) evaluation to determine whether mineral concentrations would reflect those of bone and palaeosol matrices. Normalized mass concentrations of calcium (Ca) and phosphorous (P) from the extant, fossil and palaeosol samples are given in Supplementary Table 2. Ca/P ratios of extant bone ranged from 2.68–2.8, whereas those of fossil bone ranged from 3.02–3.9. This increase in ratios reflects two processes, as evident from the mean changes in Ca and P concentrations of the five Olduvai Gorge rodents compared with modern mouse bone (Supplementary Table 2). Phosphate is depleted by 13% in the fossils, which may be owing to hydrolysis of organo-phosphate and possibly a reduction in pH from microbial activity[21]. The fossils also exhibit a 10% increase in Ca from the soil. No palaeosol had an EDS X-ray peak for P, and in all cases Ca, carbon (C) and oxygen (O) dominated their compositions (Supplementary Table 2), which corresponds to the calcium carbonate ($CaCO_3$)-based palaeosol matrices of each fossil site.

Metabolite recovery from study samples

In the first of 2 experiments relating diet to the laboratory mouse bone metabolome, from the long bone shafts of 10 genetically heterogeneous laboratory mice (UM-HET3) (Supplementary Tables 3.1a–c), we detected 25,676 features, which, after removing duplicates and compounds with no names from the pooled sample, was reduced to 2,193 metabolites for analysis. We detected 3,132 features from their diet, which was reduced to 577 metabolites for analysis. Of metabolites in the diet, 281 (48.7%) are shared with the total mouse metabolome. In the second experiment, using long bone shafts from six highly inbred mice (C57BL-6J) (Supplementary Tables 3.1c–f), we evaluated the exogenous metabolome against the ingredients of their diet (5053–PicoLab Rodent Diet 20), from which five ingredients could be related to specific metabolites (Supplementary Table 3f). There is no rationale for producing ecological profiling from exogenous metabolites derived from the artificial laboratory mouse diets. Yet, these results highlight the coupling of the metabolic profile to consumption patterns during bone formation.

From the bone fragments of 5 Olduvai Gorge Bed I rodents and 1 Bed II pig, 19,918 features were cumulatively rendered from specimens ranging in mass from 11–473 mg, which following the removal of duplicates and compounds with no names, was reduced to 2,507 metabolites for analysis (Supplementary Tables 4a–9a). The five Olduvai Gorge rodents represent four species that are still present in the vicinity of the site today. Bones from each species-matched extant representative were also analysed, rendering a cumulative 24,862 features detected and 2,600 metabolite IDs (Supplementary Tables 4a–8a).

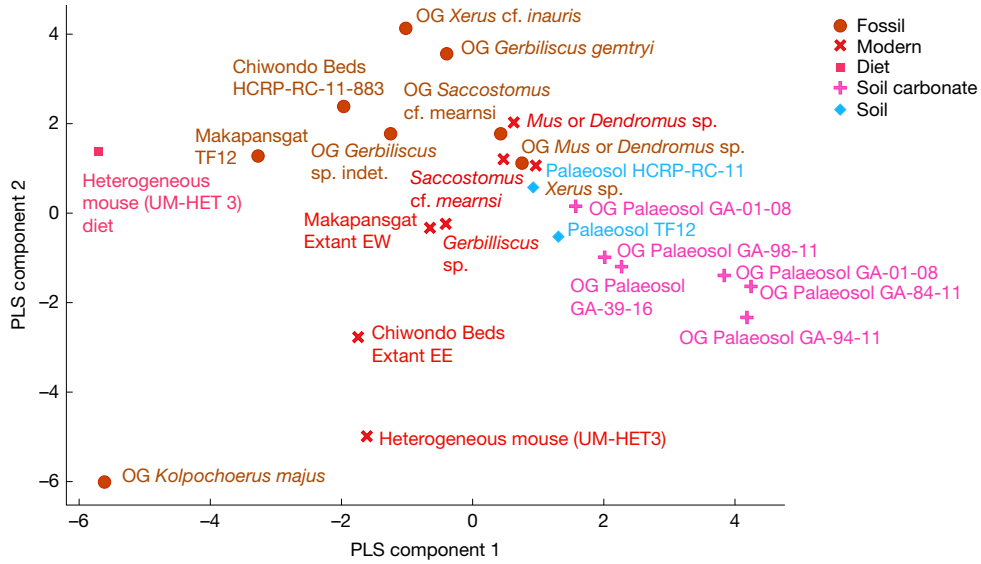

Fig. 2 | PLS-DA of the top 100 most variable metabolites. PLS-DA dimensionality reduction discriminates class labels along partial least squares (PLS) components.

Site metabolite comparisons derived from data in Supplementary Tables 4–11 are summarized in Supplementary Table 12. Endogenous metabolites shared between the four Olduvai Gorge fossils and extant species samples ranged from 50% to 100%, whereas those of exogenous metabolites shared ranged from 14.5% to 52.2%. From the dentine and cementum of the elephant sample from the Chiwondo Beds, 1,281 features were detected, 586 of which yielded metabolite IDs; and from putative bovid bone from Makapansgat, 1,489 features were detected, 694 of which yielded metabolite IDs. Endogenous and exogenous metabolites were shared with extant representatives at 66.25% and 56.6%, respectively, by the Chiwondo Beds samples, and at 53.3% and 37.8%, respectively, by the Makapansgat samples.

The metabolomes acquired from 2 dryland and 4 wetland palaeosol carbonates from Olduvai Gorge Bed I returned 39,210 features, which after removing duplicates yielded 897 metabolite IDs for comparing to the 5 rodent specimens (Supplementary Tables 4d–8d and 13). The Chiwondo Beds HCRP-RC-11 palaeosol yielded 6,580 features, resulting in 233 metabolite IDs for comparison (Supplementary Table 10d). The Makapansgat TF12 palaeosol returned 2,682 features, resulting in 1,293 metabolite IDs (Supplementary Table 11d). Supplementary Table 12 summarizes the comparisons between percentages of metabolites occurring in palaeosols against the fossils collected from these palaeosols. Olduvai Gorge rodent fossils shared 24.9–53.2% of metabolites with the palaeosols. Fossils recovered from the Chiwondo Beds and Makapansgat shared 16.0% and 61.3% of their metabolites with palaeosols obtained from their respective sites.

None of the representative extant species' bone samples were exposed to a modern soil or palaeosol. Thus, we assessed the per cent sharing of their metabolomes with the palaeosols in anticipation of null results (Supplementary Table 12). The extant Olduvai Gorge rodents shared a range of 25.7–50.5% metabolites with the palaeosols. Extant bones of taxa similar to those of the Chiwondo Beds and Makapansgat shared 14.3% and 43.8% of their metabolites with the palaeosols, respectively.

Variance in the metabolite data

Multivariate and univariate analyses consistently reveal that the major sources of variance in metabolomic profiles across samples and sites are driven by a combination of endogenous degradation products, environmental influences and metabolic residues. Principal components analysis (PCA) clearly distinguishes fossil, soil and modern samples into distinct clusters (Supplementary Figs. 8 and 9), with substantial contributions to their separation from key metabolites such as 2,4-diaminopteridine, kojic acid and hypoxanthine. Hierarchical clustering heat maps of the 100 most variable metabolites show structured groupings, further confirming category-specific biochemical signatures (Supplementary Fig. 10). Statistical tests (ANOVA and Kruskal–Wallis; Supplementary Tables 14b and 14c, respectively) identify many metabolites with significantly different abundances across categories (for example, methyl acetoacetate and myristohydroxamic acid), many of which also rank highly in the supervised partial least squares discriminant analysis (PLS-DA) model. PLS-DA of the 100 most variable metabolites reveals excellent class separation, confirming results of PCA (Fig. 2). Variable importance in projection (VIP) scores highlight a subset of metabolites that overlap with ANOVA hits that strongly drive group differences. Examples include 2,4-diaminopteridine (which also contributes in the PCA; Supplementary Table 14b) and kojic acid (significant in both ANOVA and Kruskal–Wallis; Supplementary Tables 14b and 14c, respectively). Metabolites such as kojic acid and ethyl 2,4,6-trimethoxycinnamate are key drivers of group discrimination (Supplementary Table 14d). Together, the consistent convergence of PCA, clustering, statistical testing and supervised modelling demonstrates that metabolic differences across fossil, soil and modern bone samples reflect distinct biochemical pathways shaped by degradation, environmental incorporation and species physiology.

Owl digestion and metabolite recovery

We considered that enzymes of the owl digestion system may affect the metabolomes of the bones that they consume. We evaluated this possibility in two ways. First, we compared the metabolite recovery between fossils and extant bones of the same species that were obtained by live capture (*Saccostomus* cf. *mearnsi* and *Xerus* sp.) versus extant bones of the same species that were obtained from owl pellets (*Gerbilliscus* sp. and *Mus* sp. or *Dendromus* sp.) (Table 1). The highest percentage of shared metabolites between a fossil and its extant counterpart obtained by live capture was 37.9% (*Saccostomus* cf. *mearnsi*) (Supplementary Table 5a). By contrast, the highest percentage of shared metabolites between a fossil and its extant counterpart obtained from owl pellets was 20.4% (*Gerbilliscus gentryi*) (Supplementary Table 6a).

Second, we experimented on the efficacy of metabolite recovery from the long bones of four C57BL-6J mice, in which the bones from two mice were treated with an enzyme detergent before metabolite

Table 2 | Palaeometabolome-based environmental reconstructions

Site and fossil taxon		Soil pH	Rainfall min–max (mm year^{-1})	Temperature range (°C)	Open or closed conditions	Elevation (m)	Environment
Olduvai Gorge Bed I (1.7–1.8 Ma)	Present day		250–700	14–30	Open, sunny	1,450	Semi-arid savanna
Saccostomus cf. *mearnsi*	Pleistocene	5–7	800–900	26	Open, sunny with forest shade	1,000–2,100	Seasonal dry and wet tropical biome
Gerbilliscus gentryi	Pleistocene		900–2,000	18–30	Open, sunny with forest shade	20–1,500	Seasonal dry and wet tropical biome
Xerus cf. *inauris*	Pleistocene	5–7	900	26	Open, sunny with forest shade	1,100–1,500	Seasonal dry and wet tropical biome
Mus sp. or *Dendromus* sp.	Pleistocene		1,400–2,100	28–30	Open, sunny with forest shade	1,000–2,100	Seasonal dry and wet tropical biome
Gerbilliscus sp. indet.	Pleistocene	5–7	1,000–1,200	26–29	Open, sunny with forest shade	1,000–1,650	Seasonal dry and wet tropical biome
Olduvai Gorge Bed II (1.3 Ma)	Present day		250–700	14–30	Open, sunny	1,450	Semi-arid savanna
Kolpochoerus majus	Pleistocene	7–8	1,000–1,200	20–30	Open, sunny with forest shade	1,300–2,600	Seasonal dry and wet tropical biome
Chiwondo Beds (2.4 Ma)	Present day		181 (average)	12–32	Open, sunny with forest shade	487	Seasonal dry sub-tropical biome
Elephas recki shungurensis	Pliocene	5–8	900	26	Open, sunny with forest shade	400–650	Seasonal dry and wet tropical biome
Makapansgat (3 Ma)	Present day		600 (average)	6–29 average	Open, sunny with forest shade	1,440	Grassland savanna with trees and bush
Bovidae	Pliocene	6–6.5	800–1200	26–30	Open, sunny with forest shade	650–1,500	Seasonal dry and wet tropical biome

extraction. The total number of metabolites with IDs recovered from the untreated samples was 70, whereas only 9 metabolites with IDs were recovered from the enzyme-treated samples (Supplementary Table 3g).

Endogenous mammalian metabolites

The extent to which endogenous metabolites are shared between the fossil and extant species samples is reported in Supplementary Table 12; it represents the proportions of shared canonical pathways, biological functions and gene networks presented in Supplementary Tables 4b–11b identified in ingenuity pathway analysis (IPA). These depict a variety of normal mammalian endogenous functions and disease states that describe the biology of each animal. The most common IPA-defined biological functions relate to amino acid metabolism, cell death and survival, carbohydrate metabolism, cellular growth and proliferation, organismal development, molecular transport, energy production, lipid metabolism, vitamin and mineral metabolism, the cell cycle, and developmental disorders, some of which are shared among the fossil specimens.

Exogenous non-mammalian metabolites

Although IPA maps IDs to endogenous and exogenous categories, it only provides pathway, biological function and network analyses for endogenous metabolites. There is currently no database where exogenous metabolites may be queried for ecological inferences. We present initial entries for such a database in Supplementary Tables 4–11.

The reconstructed environmental conditions derived from each fossil according to palaeontological site are summarized in Table 2. Acknowledging variability and some outliers in Supplementary Tables 4k–8k, 10k and 11k, in the main Early Pleistocene conditions at eastern African Olduvai Gorge Bed I and II sites and at the southern African Makapansgat site were wetter, minimum temperatures were higher, and the landscape contained more forest shade than in the present day, consistent with a mixed seasonally dry and wet tropical biome. The reconstructed conditions of the central African Chiwondo Beds site indicate a wetter environment consistent with a mixed seasonally dry and wet tropical biome.

Discussion

Metabolite preservation

Provided that the depositional environment is not diagenetically extreme, fossils more than 150,000 years old have been shown to harbour endogenous and exogenous amino acids and lipids[22]. Haem-containing compounds detected from dinosaur bone[23] and eggshell[24] have been found to enhance the resistance to protein degradation by haem-derived iron-catalysed non-enzymatic cross-linking of structural molecules[25]. Fourier transform infrared spectroscopy, transmission electron microscopy and time-of-flight secondary ion mass spectrometry (ToF-SIMS) of collagen in dinosaur bone is conclusive (in ref. 26, for example), as its preservation potential is fostered by resistance to hydrolysis[27]. Peptide sequence analyses and immunological data similarly demonstrate that a variety of bone matrix and blood vessel proteins survive in 80 million year-old dinosaur samples. Raman microscopy of fossils from the Phanerozoic eon has revealed that oxidizing diagenetic environments permit specific protein cross-linking, rendering intact endogenous peptide bonds that persist in fossil mineralized tissues[28].

In all studies of metabolite stability, the matrix is either aqueous at room temperature, cooled, frozen or dried and exposed to air. These conditions differ from those used in the recovery of metabolites from hard tissues, particularly of the fossils we present here, which therefore requires an inferential explanation.

Metabolites located in the mineralized extracellular matrix may derive from two sources. The biological processes of overlying osteoblasts and incorporating osteocytes at forming and mineralizing fronts is one source of metabolites released into the extracellular space. A second, more abundant source of metabolites must be driven to the extracellular space from the vasculature during bone formation, which at forming and mineralizing fronts contains a rich capillary network[29]. By osmotic diffusion and transport mechanisms, capillaries provide the cellular milieu with metabolic requirements and metabolites[30],

thus metabolite infusion into this space appears to be derived from the free circulation, where the osteoblast cell-surface layer does not provide a barrier function. Tight junctions in extensive, belt-like cell-circumscribing arrangements (such as zonula occludens) similar to those that occur in epithelial cell layers do not form in osteoblasts, but whether they form a complete barrier is moot. Cultured primary osteoblasts form a monolayer with tight junctions, and the formation of a barrier has been suggested[31]. However, an investigation of osteoblasts on natural bone substrates found that tight junction contact density is relatively low[32]. Another cell culture experiment concluded that tight junctions were situated at vesicular trafficking points, and that when cells were otherwise confluent in a monolayer, the tight junctions were distributed only in a punctate manner that would not render a barrier function[33].

Bone is formed of a carbonate-substituted hydroxyapatite mineral intermingling with the major, large and fibrillar structural protein collagen, which are known to be preserved intact in fossils of Plio-Pleistocene age as examined here[34]. Polarized light microscopy of the fossil specimens investigated in this study demonstrated positive birefringence typical of preserved bone microstructure in these Plio-Pleistocene fossils. We theorize that without evidence of permineralization effects, such polarized light signals derive from reasonably intact collagen because apatitic mineral has a very low birefringence, which is overwhelmed by that of the collagen. To confirm this result, we performed proteomics on the precipitate from the metabolomics preparations of four rodent fossils from Olduvai Gorge (M-D, Sm, Gg and Xi). Collagen peptide and related IDs that describe collagen matrices were detected from M-D and Sm (Supplementary Table 15 and Supplementary Figs. 5 and 6).

If polarized light microscopy of fossil specimens indicated brightness attributable to collagen, then we hypothesize that the preservation of other biomolecules as reported here is expected. Although this hypothesis remains unconfirmed, and although collagen peptides were detected in only two of four specimens examined, the presence of metabolites in the specimens is irrefutable. From first principles, we detail how we believe these metabolites are incorporated into protective nanoscopic niches of bone (Methods). We regard the nanocompartments as having metabolite preservation potential if two conditions are met: (1) circulating metabolites can enter the spatially constrained niche occupied by interstitial water; and (2) these compartments are not readily connected to an open system in bone subject to diagenesis (that is, they are not exposed to air or mobile water) and thus are shielded from diagenesis (Fig. 3).

There are several non-exclusive pathways for the degradation of organic compounds in bone, but we suggest that if a bone's protective mineral has maintained the fibrous collagenous extracellular matrix, then associated nanocompartments and metabolites are also likely to remain intact. This is consistent with biomolecular preservation and staining typical of oxidative diagenetic environments that render brown hues in histology[28], as was often observed among the fossils in this study, in addition to some collagen that was presumed to be transmitting birefringent white light.

Although the conditions are different, metabolite preservation from plant resin[35] and tobacco[36] residues in archaeological contexts demonstrates a specific resistance to their degradation. In our study a *t*-test finds no significant difference between the average molecular mass in the fossil specimens and their extant skeletonized counterparts (Fig. 4 and Supplementary Table 16a). Yet, the average molecular mass in the laboratory mouse metabolomes is about 75 Da higher. It is likely that metabolites from bone cells included in the metabolite extraction are contributing to this larger molecular mass fraction; for example, the average molecular mass of 113 metabolites detected from a yeast cell[37] is 269 Da, which is within the narrow range given for the laboratory mouse metabolomes (Fig. 4).

The rat bone has a cellular density of approximately 60,000 mm^{-3} (ref. 38), and given the negative body mass dependence of the cell density, we expect the value for mouse to be around 75,000 mm^{-3}. The 20 mg bone samples from the extant laboratory mouse are estimated to occupy approximately 1 mm^3. Thus, metabolites from about 75,000 cells will be represented in each bone's extract. Metabolomics[39] analyses of powdered extant mouse femurs demonstrate that cells contribute a metabolite solute to the extraction solvent. Further research is required to more fully understand the extent to which degradation occurs in fossil and extant skeletonized bone devoid of cells.

Insights on the endogenous metabolome

Aside from the summary of normal mammalian endogenous functions and disease states described above, IPA analyses of the molecular physiological machinery responsible for the metabolome of each animal are detailed in Supplementary Tables 4b–11b, with a list of canonical pathways, functions, diseases and gene networks. Associations with genes related to oestrogen biosynthesis and signalling suggest that both Olduvai Gorge gerbils (specimens Gg and Gi; Supplementary Tables 6b and 7b, respectively) as well as the ground squirrel (specimen Xi; Supplementary Table 8b) were female, as was the Makapansgat bovid (sample TF12; Supplementary Table 11b). On the basis of oestrone detected in specimens Gg and Xi, we are less confident, relying only on the higher concentration of this form of oestrogen in females than in males. However, our confidence is higher regarding specimens Gi and TF12, in which placental oestriol and luteinizing hormone are indicated. Notes regarding sex hormones are shown adjacent to the gene network in each supplementary table referenced above.

The results from the Olduvai Gorge ground squirrel, the Chiwondo Beds elephant and the Makapansgat bovid also present an opportunity to connect the endogenous and exogenous metabolomes. Associations with genes related to proinflammatory cytokines in data from these individuals may be the result of the *Trypanosoma brucei* infection identified in each of their exogenous metabolomes (Supplementary Tables 8k, 10k and 11k), which is also revealed in proteomics analysis of the ground squirrel specimen Xi (Supplementary Fig. 7).

Endogeneity assessment

We considered that taphonomic research demonstrating the owl digestion of rodent bone might contribute to a metabolite signal. Rodents excavated from FLK N1 layer M3 and M2 were deposited as pellets by Verreaux's eagle-owl (*Bubo lacteus*), whereas those from FLK N1 layer M1 were deposited by the spotted eagle-owl (*Bubo africanus*)[5] (Table 1). Unlike other birds, owls lack a 'crop' to store and digest food slowly. Instead, non-digestible contents (such as bone and fur) are formed as a pellet in the gizzard and regurgitated after several hours, and thus not excreted through the digestive tract (owls cannot eat again until they eject this pellet). Owls have a higher pH in their 'true' stomach (proventriculus) than other birds, but experiments have confirmed that its acids may mildly corrode bone surfaces. However, experimental taphonomic research indicates no more surface damage than might occur during normal bone weathering[40,41]. A two-proportion *z*-test of the percentage of shared metabolites between the fossil of *Saccostomus* cf. *mearnsi* and its extant counterpart obtained by live capture versus the fossil of *Gerbilliscus gentryi* and its extant counterpart obtained in an owl pellet reveals a highly significant loss of shared metabolites as a result of it being subject to the owl's digestion ($P < 0.01$; Supplementary Table 16b). The possibility of metabolites intruding into the bone matrix attributable to digestion is thus insignificant. This assessment was mirrored by our enzymatic laboratory test of fresh mouse bone in which the metabolite recovery was diminished over that of bones that were not subject to enzymatic digestion.

The potential incorporation of metabolites excreted by the gut microbiome may also be considered. Given our supposition that metabolites are incorporated into mineralizing surfaces, we expect only metabolite loss, and no metabolite gain. Further, the avian proventriculus has a reduced bacterial diversity compared with the gut[42],

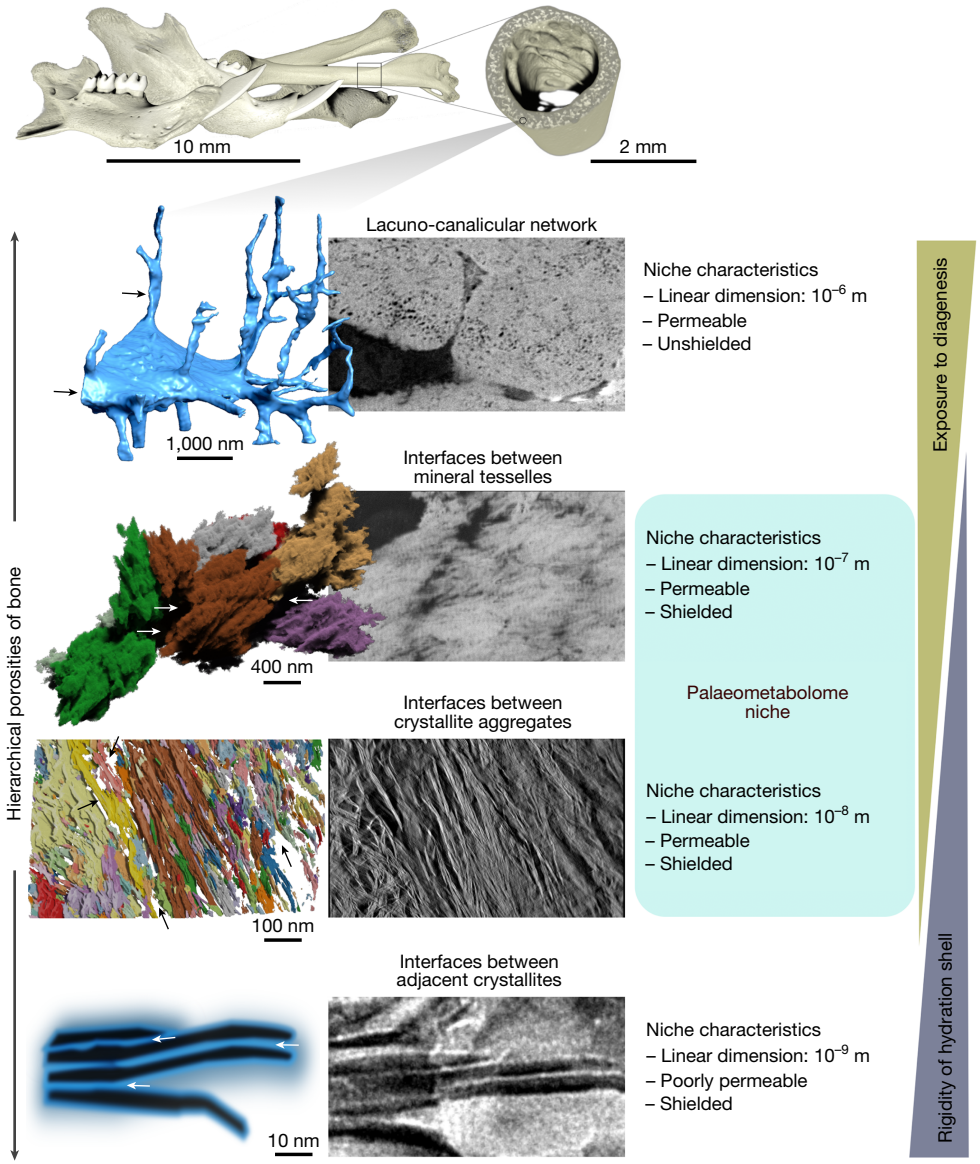

Fig. 3 | Bone ultrastructure and metabolite niches. Within the hierarchical porosities of mineralized tissues, the niche that is suitable for palaeometabolome preservation is both permeable for transudate and shielded from diagenesis.

the former being mainly responsible for acid and enzymatic break down of food, which the bones do not experience. Among the Olduvai Gorge rodent fossils, only the bone of *Saccostomus* cf. *mearnsi*, which was obtained from an owl pellet, contained a bacterial xenobiotic metabolite (6-hydroxyhexanoic acid; Supplementary Table 5k). However, species obtained by live capture (*Saccostomus* cf. *mearnsi*, *Gerbilliscus* sp. and *Xerus* sp. (Supplementary Tables 5a, 7a and 8a, respectively)) also contain this metabolite. Thus, it is more likely that the presence of xenobiotic metabolites derives from their incorporation into the mineralizing tissues of the animals independent of their passage through owls.

An endogeneity assessment of palaeosols' metabolite contribution to the fossils was also considered. In testing the assumption of contamination by palaeosols from the three palaeontological sites, we discovered them to be independent repositories of metabolites detected from the fossils (Supplementary Table 12). The five rodent fossils from Olduvai Gorge share an average of 41.1% of total metabolites with the palaeosol. Yet, their extant counterparts, which had no contact with soil, share 40.4% of total metabolites. At the Chiwondo Beds, the fossil/extant proportions are 16.0/14.3. At Makapansgat, they are 61.3/43.8, respectively, the latter offset perhaps due to the sampled extant African bovid, while having a South African distribution, nevertheless originating in Malawi. The palaeosols at each palaeontological site are calcium carbonate-based (Supplementary Table 2). During natural carcass degradation, decomposition fluids containing metabolites (analogous to those that could have been sequestered in bone crystallite niches antemortem) seep into the soil. Loamy soils feature a broad size spectrum of porosities some of which can sequester and shield organic compounds originating from numberless decomposition events over time. We suspect that the crystalline matrices of these soils harbour metabolites from the environment, which are taken up and protected during their mineralization: it is not the soil compounds that contaminate the fossils, but rather decomposition compounds that contaminate the soils.

Insights on the exogenous metabolome

The various taphonomic, palynological and geological approaches taken to reconstruct the environment at Olduvai Gorge present a reasonably vivid macro-scale rendering of the environment in the Early Pleistocene[3–5,43]. This depiction ends where interpretations of the

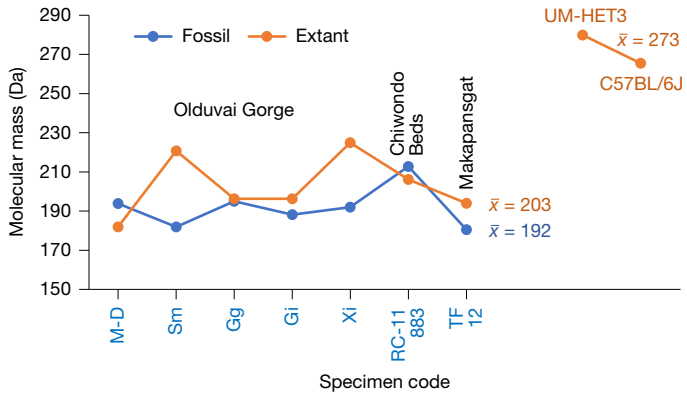

Fig. 4 | Average metabolite molecular masses of extant and fossil hard tissues. Molecular masses of metabolites extracted from fossils from five Olduvai Gorge rodents, a Chiwondo Beds elephant and a Makapansgat bovid. Fossil specimens are plotted together with their corresponding extant representatives and two laboratory mouse strains. Sample grand means ($\bar{x}$) are given for each category.

palaeometabolome begin, by detailing the exogenous metabolites derived from fossil bones, and from these the inferred attributes of soil, atmosphere, sun exposure, potential species names of organisms and the habitat and food preferences of the animals that lived there. These metabolites and their sources are listed in Supplementary Tables 4k–8k, 10k and 11k, which we summarize in Table 2 and generally remark upon here.

The exogenous metabolites recovered from the Olduvai Gorge fossils are mainly those of soil bacteria *Escherichia* and *Streptomyces*. Both are widely distributed in soils of the world. *Escherichia* is a common member of open habitat soil microbiomes[44] that contribute to plant growth. *Streptomyces* is also widely distributed in soils around the world[45] and its presence in the study samples is probably attributable to its participation in decaying vegetation[46] that supports the notion of a woodland forest floor. *Streptomyces* spp. also have collagenase-producing capabilities[2], which will have contributed to the decay of bone.

Metabolites of fungi generally indicate mesic conditions: periods of high humidity, little or no wind at night, and generally temperatures of 16 °C and above[47–49]. Monocotyledons such as *Asparagus*[50] and *Aloe*[51] genera prefer well-drained, loamy–sandy soils of various textures with pH in the range of 5–8, and open sunny conditions. Other genera, such as *Aframomum*[52] and *Piper*[53], prefer shady and humid forest conditions. Environmental conditions of the monocotyledons generally also apply to the list of herbaceous dicotyledons. Around 400–2,100 mm annual rainfall sustains the ecology for both monocotyledon and herbaceous dicotyledon flowering plant categories (Supplementary Tables 4k–8k, 10k and 11k).

No woody dicotyledon plant species were identified that survive on semi-arid xerophytic forests, woodlands or savannas. The flora given in Supplementary Tables 4k–8k, 10k and 11k represent mesic and mixed eurybiomic thicket-woodland and fresh groundwater woodland or bushland on well-drained loamy soils such as *Kigelia africana*[54], most species of which do not occupy the dominantly semi-arid grassland, acacia and Commiphora scrubland of Olduvai Gorge today[4].

The ground squirrel has a metabolite unique to *T. brucei*, the trypanosome responsible for sleeping sickness in humans following the bite from an infected tsetse fly. This disease has been traced to early Plio-Pleistocene stages of human evolution[55], consistent with tsetse living in tropical African gallery forest, thicket, miombo woodland, mopane woodland and grassland today, which typically have a temperature range[56] of around 16–32 °C. There are many wildlife reservoirs for this parasite, including squirrels, ungulates and elephants[57], which is reflected in our fossil sample.

Estimation of the palaeoecology from the *Kolpochoerus majus* palaeometabolome derived from Olduvai Gorge Bed II was undertaken in much the same way as for the rodent fossils, except that it was restricted to a comparison of the annotated exogenous metabolites in Supplementary Table 9c, with isotope-informed exogenous metabolites based on evidence attributed to this species[58] (Supplementary Table 9d). Although the two palaeoenvironmental reconstructions contain some minor differences, the reconstruction presented in Table 2 was based on the isotope-informed analysis in Supplementary Table 9d.

Overall, our Olduvai Gorge palaeometabolomes support the diversity of habitats identified in the palaeoenvironmental reconstructions of the freshwater woodland and grasslands of Olduvai Gorge Bed I[3–5], and the dry woodlands and marshy areas of Olduvai Gorge Upper Bed II[6].

Palaeometabolomics may parse an ecogeographic context, as determined by our selection of regionally specific plant categories that differentially characterize the central African Chiwondo Beds and southern Makapansgat sites. This includes the sub-tropical woodland and lakeshore habitats of the Chiwondo Beds[13,14,59] and the moist mosaic bushland of Makapansgat[60], consistent with reconstructions in Table 2.

Despite the precise nature of mass spectrometry-based palaeometabolomic IDs, the basic science requires advancement. Searches for medicinal plant metabolites do not canvass all available species in an environment and therefore a vast exogenous metabolite inventory remains unexamined in the study sites. For instance, many species listed in Supplementary Tables 4k–8k, 10k and 11k are native to other African and/or world regions, such as Asian *Croton tiglium*. Yet, this genus has many African natives, including some in the African study regions today. Metabolite references to *Asparagus officinalis*, although it is a native species in northern Africa, are more likely to be due to the consumption of *Asparagus africanus*, broadly distributed among acacia woodlands of eastern and central Africa. These other native species may have lived in the Pleistocene of the eastern Serengeti, or the associated metabolite could have been from a genus or species whose metabolome has not been examined. At this time, we believe that information linking metabolites to molecular ecological inferences is only just now sufficient to prime the field. Further exogenous metabolomics research will broaden basic science initiatives beyond the limits of biomedical interests in medicinal plants so that we may characterize the metabolomes of many modern plants and environments of interest to palaeoecologists. Despite being liberal in our current approach to glean as much information as possible from an undeveloped database, such that inferences that we have reached may be critiqued, there appears to be sufficient explanatory value in the palaeometabolome to corroborate recent palaeoecological reconstructions, adding to these reconstructions fine-grained specifics that potentially approach our ability as field ecologists to describe the characteristics of a modern environment.

Online content

Any methods, additional references, Nature Portfolio reporting summaries, source data, extended data, supplementary information, acknowledgements, peer review information; details of author contributions and competing interests; and statements of data and code availability are available at https://doi.org/10.1038/s41586-025-09843-w.

1. Zhang, A., Sun, H., Wang, P., Han, Y. & Wang, X. Recent and potential developments of biofluid analyses in metabolomics. *J. Proteomics* **75**, 1079–1088 (2012).
2. Endo, A., Murakawa, S. & Shimizu, H. Purification and properties of collagenase from a *Streptomyces* species. *J. Biochem.* **102**, 161–170 (1987).
3. Ashley, G. M. et al. Paleoenvironmental and paleoecological reconstruction of a freshwater oasis in savannah grassland at FLK North, Olduvai Gorge, Tanzania. *Quat. Res.* **74**, 333–343 (2010).
4. Barboni, D. et al. Phytoliths infer locally dense and heterogeneous paleovegetation at FLK North and surrounding localities during upper Bed I time, Olduvai Gorge, Tanzania. *Quat. Res.* **74**, 344–354 (2010).
5. Fernández-Jalvo, Y. et al. Taphonomy and palaeoecology of Olduvai Bed-I (Pleistocene, Tanzania). *J. Hum. Evol.* **34**, 137–172 (1998).

6. Kovarovic, K., Slepkov, R. & McNulty, K. P. Ecological continuity between Lower and Upper Bed II, Olduvai Gorge, Tanzania. *J. Hum. Evol.* **64**, 538–555 (2013).
7. Euw, S. V et al. Organization of bone mineral: the role of mineral–water interactions. *Geosciences* **8**, 466 (2018).
8. Brown, J. H., Gillooly, J. F., Allen, A. P., Savage, V. M. & West, G. B. Toward a metabolic theory of ecology. *Ecology* **85**, 1771–1789 (2004).
9. Gillooly, J. F., Brown, J. H., West, G. B., Savage, V. M. & Charnov, E. L. Effects of size and temperature on metabolic rate. *Science* **293**, 2248–2251 (2001).
10. West, G. B., Woodruff, W. H. & Brown, J. H. Allometric scaling of metabolic rate from molecules and mitochondria to cells and mammals. *Proc. Natl Acad. Sci. USA* **99**, 2473–2478 (2002).
11. Padian, K. & Ricqlès, A. D. Inferring the physiological regimes of extinct vertebrates: methods, limits and framework. *Phil. Trans. R. Soc. B* **375**, 20190147 (2020).
12. Köhler, M., Marín-Moratalla, N., Jordana, X. & Aanes, R. Seasonal bone growth and physiology in endotherms shed light on dinosaur physiology. *Nature* **487**, 358–361 (2012).
13. Lüdecke, T. et al. Persistent C3 vegetation accompanied Plio-Pleistocene hominin evolution in the Malawi Rift (Chiwondo Beds, Karonga Basin, East African Rift System). *J. Hum. Evol.* **90**, 163–175 (2016).
14. Schrenk, F., Bromage, T. G., Sandrock, O. & Gorthner, A. Paleoecology of the Malawi Rift: Vertebrate and invertebrate faunal contexts of the Chiwondo Beds, northern Malawi. *J. Hum. Evol.* **28**, 59–70 (1995).
15. Huber, B., Larsen, T., Spengler, R. N. & Boivin, N. How to use modern science to reconstruct ancient scents. *Nat. Hum. Behav.* **6**, 611–614 (2020).
16. Badillo-Sanchez, D., Davies-Barrett, A. M., Ruber, M. S., Jones, D. J. L. & Inskip, S. A. Archaeometabolomics characterizes phenotypic differences in human cortical bone at a molecular level relating to tobacco use. *Sci. Adv.* **10**, eadn9317 (2024).
17. Enlow, D. H. *Principles of Bone Remodeling* (Charles C. Thomas, 1963).
18. Albuquerque, U. P., Ramos, M. A. & Melo, J. G. New strategies for drug discovery in tropical forests based on ethnobotanical and chemical ecological studies. *J. Ethnopharmacol.* **140**, 197–201 (2012).
19. Balunas, M. J. & Kinghorn, A. D. Drug discovery from medicinal plants. *Life Sci.* **78**, 431–441 (2005).
20. Sumner, L. W., Mendes, P. & Dixon, R. A. Plant metabolomics: large-scale phytochemistry in the functional genomics era. *Phytochemistry* **62**, 817–836 (2003).
21. Wiemann, J. *A Fundamental Exploration of the Interactions Between Minerals and Life's Building Blocks in Deep Time*. PhD thesis, Yale Univ. (2021).
22. Colleary, C., Lamadrid, H. M, O'Reilly, S. S, Dolocan, A. & Nesbitt, S. J Molecular preservation in mammoth bone and variation based on burial environment. *Sci. Rep.* **11**, 2662 (2021).
23. Schweitzer, M. H. et al. Heme compounds in dinosaur trabecular bone. *Proc. Natl Acad. Sci. USA* **94**, 6291–6296 (1997).
24. Wiemann, J. et al. Dinosaur origin of egg color: oviraptors laid blue-green eggs. *PeerJ* **5**, e3706 (2017).
25. Boatman, E. M. Mechanisms of soft tissue and protein preservation in *Tyrannosaurus rex*. *Sci. Rep.* **9**, 15678 (2019).
26. Bertazzo, S. et al. Fibres and cellular structures preserved in 75-million–year-old dinosaur specimens. *Nat. Commun.* **6**, 7352 (2015).
27. Yang, J., Kojasoy, V., Porter, G. J. & Raines, R. T. Pauli exclusion by n→π* interactions: implications for paleobiology. *ACS Cent. Sci.* **10**, 1829–1834 (2024).
28. Wiemann, J. et al. Fossilization transforms vertebrate hard tissue proteins into N-heterocyclic polymers. *Nat. Commun.* **9**, 4741 (2018).
29. Filipowska, J., Tomaszewski, K. A., Niedźwiedzki, Ł, Walocha, J. A. & Niedźwiedzki, T. The role of vasculature in bone development, regeneration and proper systemic functioning. *Angiogenesis* **20**, 291–302 (2017).
30. Godwin, L., Tariq, M. A. & Crane, J. S. in *StatPearls* (StatPearls Publishing, 2022).
31. Wongdee, K. et al. Osteoblasts express claudins and tight junction-associated proteins. *Histochem. Cell Biol.* **130**, 79–90 (2008).
32. Weinger, J. M. & Holtrop, M. E. An ultrastructural study of bone cells: The occurrence of microtubules, microfilaments and tight junctions. *Calcif. Tissue Res.* **14**, 15–29 (1974).
33. Prêle, C. M., Horton, M. A., Caterina, P. & Stenbeck, G. Identification of the molecular mechanisms contributing to polarized trafficking in osteoblasts. *Exp. Cell. Res.* **282**, 24–34 (2003).
34. Saitta, E. T. Cretaceous dinosaur bone contains recent organic material and provides an environment conducive to microbial communities. *eLife* **8**, e46205 (2019).
35. Brettell, R. C. et al. 'Choicest unguents': molecular evidence for the use of resinous plant exudates in late Roman mortuary rites in Britain. *J. Archaeolog. Sci.* **53**, 639–648 (2015).
36. Zimmermann, M. et al. Metabolomics-based analysis of miniature flask contents identifies tobacco mixture use among the ancient Maya. *Sci. Rep.* **11**, 1590 (2021).
37. Li, Z. et al. Single-cell mass spectrometry analysis of metabolites facilitated by cell electro-migration and electroporation. *Anal. Chem.* **92**, 10138–10144 (2020).
38. Bromage, T. G., Goldman, H. M., McFarlin, S. C., Perez-Ochoa, A. & Boyde, A. Confocal scanning optical microscopy of a 3-million-year-old *Australopithecus afarensis* femur. *Scanning Microsc.* **31**, 1–10 (2009).
39. Welhaven, H. D. et al. The cortical bone metabolome of C57BL/6J mice is sexually dimorphic. *J. Bone Miner. Res.* **6**, e10654 (2022).
40. Denys, C., Reed, D. N. & Dauphin, Y. Deciphering alterations of rodent bones through in vitro digestion: an avenue to understand pre-diagenetic agents? *Minerals* **13**, 124 (2023).
41. Fernandez-Jalvo, Y., Andrews, P., Sevilla, P. & Requejo, V. Digestion versus abrasion features in rodent bones. *Lethaia* **47**, 323–336 (2014).
42. Feye, K. M., Baxter, M. F. A., Tellez-Isaias, G., Kogut, M. H. & Ricke, S. C. Influential factors on the composition of the conventionally raised broiler gastrointestinal microbiomes. *Poultry Sci.* **99**, 653–659 (2020).
43. Ashley, G. M. et al. A spring and wooded habitat at FLK Zinj and their relevance to origins of human behavior. *Quat. Res.* **74**, 304–314 (2010).
44. Elsas, J. D. V., Semenov, A. V., Costa, R. & Trevors, J. T. Survival of *Escherichia coli* in the environment: fundamental and public health aspects. *ISME J.* **5**, 173–183 (2011).
45. Valdezate, S. in *Encyclopedia of Infection and Immunity* Vol. 1 (ed. Rezaei, N.) 589–613 (Elsevier, 2022).
46. Loria, R., Bukhalid, R. A., Fry, B. A. & King, R. R. Plant pathogenicity in the genus *Streptomyces*. *Plant Dis.* **81**, 836–846 (1997).
47. Egidi, E. et al. A few Ascomycota taxa dominate soil fungal communities worldwide. *Nat. Commun.* **10**, 2369 (2019).
48. Velásquez, A. C., Castroverde, C. D. M. & He, S. Y. Plant and pathogen warfare under changing climate conditions. *Curr. Biol.* **28**, R619–R634 (2018).
49. Money, N. P. in *The Fungi* (eds Watkinson, S. C., Boddy, L. & Money, N. P.) 1–36 (Academic Press, 2016).
50. Fern, K. *Asparagus africanus*. *Tropical Plants Database* tropical.theferns.info/viewtropical.php?id=Asparagus+africanus (2025).
51. Newton, L. E. in *Aloes: The Genus Aloe Medicinal and Aromatic Plants—Industrail Profiles* (ed. Reynolds, T.) 1–16 (CRC Press, 2004).
52. Harris, D. J. & Wortley, A. H. *Monograph of Aframomium (Zingiberaceae)*, Vol. 104, 1–204 (American Society of Plant Taxonomists, 2018).
53. Fern, K. *Piper capense*. *Tropical Plants Database* tropical.theferns.info/viewtropical.php?id=Piper+capense (2025).
54. Fern, K. *Kigelia africana*. *Tropical Plants Database* tropical.theferns.info/viewtropical.php?id=Kigelia+africana (2025).
55. Labrecht, F. L. Aspects of evolution and ecology of tsetse flies and trypanosomiasis in prehistoric African environments. *J. Afr. Hist.* **5**, 1–24 (1964).
56. Pollock, J. N. (ed.) *Training Manual for Tsetse Control Personnel, Vol. 2. Ecology and Behaviour of Tsetse* (Food and Agriculture Organization of the United Nations, 1982).
57. Kasozi, K. I. et al. Epidemiology of Trypanosomiasis in wildlife—implications for humans at the wildlife interface in Africa. *Front. Vet. Sci.* https://doi.org/10.3389/fvets.2021.621699 (2021).
58. Souron, A. in *Ecology, Conservation and Management of Wild Pigs and Peccaries* (eds Melletti, M. & Meijaard, E.) 29–38 (Cambridge Univ. Press, 2017).
59. Sandrock, O., Kullmer, O., Schrenk, F., Juwayeyi, Y. M. & Bromage, T. G. in *Hominin Environments in the East African Pliocene: An Assessment of the Faunal Evidence* (eds Bobe, R. Alemseged, Z. & Behrensmeyer, A. K.) 315–332 (Springer, 2007).
60. Reed, K. E. et al. in *African Paleoecology and Human Evolution* (eds Reynolds, S. C. & Bobe, R.) 66–81 (Cambridge Univ. Press, 2022).

Methods

Analysis of bone mineral niches

The predominant mineral phase of bone is a carbonate-substituted hydroxyapatite mineral integrated within an organic extracellular matrix consisting mainly of the large, structural fibrillar protein collagen, which fossils of the Pleistocene age such as examined here and older are known to preserve intact[34]. Brightness in polarized light microscopy putatively indicates the presence of collagen (Extended Data Figs. 1–5 and Supplementary Figs. 1 and 2), which proteomics analysis positively identified in two of four samples tested (Supplementary Figs. 5 and 6). Beyond the identification of molecular collagen, bone is hierarchically constructed at a considerable number of levels, from its macroscopic morphology at one extreme, to the nanoscopic domain of mineral platelets, needles, and unit cells at the other[61–63]. For biomolecules such as circulating metabolites to reach the extracellular compartment in mineralizing bone to be preserved intact, we considered that they must be protected by a 'solid' mineral phase.

To further examine this notion of bone mineral hierarchical structure being protective of circulating metabolites, we considered that carbonated hydroxyapatite in bone (and otherwise) possesses an ion-exchangeable surface in aqueous environments[64,65] that can readily bind and exchange ions and molecules[66]. In the in vivo environment, it is now apparent that this adsorption is not limited to bone-specific and locally produced ions and molecules, but it also includes circulating metabolites that readily enter bone through its interstitial fluid. The adsorption is mediated predominantly by electrostatic interactions and the formation of coordination complexes with surface ions of the mineral phase[66]. The adsorption of metabolites to the surface of mineral crystallites, coupled with retention of water into bone's hierarchical structure, results in entrapment of the metabolites within a continuum of structural niches spanning size scales from micrometres to nanometres. For a niche to be suitable for long-term metabolite entrapment and preservation in bone, on the palaeology timescale, it must be accessible to the interstitial fluid (to allow metabolites in), and it must also be shielded from taphonomic processes (to prevent metabolite loss). The broader and larger the scale of structural organization in bone, the more permeable the organic–inorganic interfaces are for metabolites, yet at the same time also for subsequent metabolite degradation and diagenetic events. Conversely, at the finer scale of bone mineral structure where there is generally less permeability, metabolites may be sequestered and then shielded from degradation and loss—and thus remain detectable—as we have discovered in this study. Therefore, we considered the continuum of three-dimensional (3D) sub-micrometre niches that can possibly harbour the palaeometabolome, according to their permeability and scale (Fig. 3).

Lacuno-canalicular network, 10^{-6} m scale

Based on (palaeo)histological studies, the lacuno-canalicular network is easily accessible to both metabolites and taphonomic agents such as microbes and humic substances[67,68]. Numerous studies have demonstrated that the lacuno-canalicular network is easily infiltrated by microorganisms like the hyphae of filamentous fungi[69] and by bacteria[70], and can serve as conduit for diagenetic processes. Enzymatic degradation and modification of the local microenvironment along the microbial ingress degrades collagen and non-collagenous proteins, resulting in reprecipitation of mineral phases and the loss of pristine organic–inorganic interfaces[70,71]. Although the preservation of collagen in parts of the sample suggests that the diagenetic degradation was incomplete, allowing the preservation of some sub-micrometre structures, we view this lacuno-canalicular network niche as being of limited reliability for palaeometabolome preservation, dependent on the burial conditions.

Mineral tesselle interface, 10^{-7} m scale

In living bone, mineralization begins from quasi-regularly spaced mineralization foci[72,73] dispersed within a fibrous collagenous extracellular matrix. Mineral foci grow within the organic matrix to eventually pack into a 3D, space-filling array of similarly structured morphologies geometrically approximating prolate ellipsoids about 1 µm in size, in a process termed crossfibrillar mineral tessellation[72]. Even mature mineral ellipsoids, called tesselles, have persistent discrete organic boundaries that do not exceed 100–200 nm. Such boundaries are likely to contain residual mineralization-inhibiting non-collagenous proteins or peptides and inhibitory small biomolecules that presumably impede complete fusion of the tesselles, thus providing a 3D tessellation pattern that imparts unique mechanical properties to bone[73,74]. This nanometre-scale (100–200 nm) compartment is thus a probable niche for palaeometabolome preservation.

Between crystallite groups, 10^{-8} m scale

Gently twisted aggregates of stacked hydroxyapatite crystallites splay and merge throughout the continuous collagenous matrix[62,75]. Neighbouring aggregates envelope spaces that are, on average, about 20 nm wide and linear in the in-plane view, or 30–40 nm wide and lacy in the out-of-plane view[75]. Continuous with the collagen fibrils is an extended network of small proteoglycans (small leucine-rich proteoglycans) with chains of dermatan and chondroitin sulfate[76]. These charged proteoglycan chains can be up to 30 nm in length[77] and their networks can bridge this inter-crystallite aggregate niche, being on the order of magnitude of several thousands of cubic nanometres. Experimental evidence demonstrates an ionic dependence on cohesive forces between nanointerfaces of native bone suggesting that there are electrostatically mediated interactions between the charged proteoglycans and mineral surfaces in a hydrated environment[78]. Furthermore, in situ measurements of bone zeta potential suggest that the long-range (>10 nm) electrostatic effects on the surface are predominantly from charged protein groups[79]. Such a crowded molecular environment with an abundance of charged and polar residues can sequester metabolites, making this compartment a probable protected palaeometabolome preservation niche.

Between crystallites, 10^{-9} m scale

We next considered this finest niche, which is uniformly sandwiched between congruent surfaces of adjacent hydroxyapatite crystallites and does not exceed a few nanometres in width. These uniform confined spaces are typically visible in thin sections of bone viewed by transmission electron microscopy[80–82]. Hydrated bone mineral bears a surface charge (−50 mV) and a corresponding surface potential gradient. The extent of the surface potential gradient is defined by complexation (through chemisorption) of water dipoles with undercoordinated surface ions. From simulations of hydroxyapatite electrostatics at physiological conditions, it is predicted that bone mineral crystallites have a relatively thick (2.7 nm) and strongly bound hydrated layer on their surfaces[7]. This layer thickness, known collectively as the Debye length, is composed of the Stern–Helmholtz and electric double layer—a dense ionic halo that acts as the interface in between the charged crystallite surface and the labile interstitial fluid. An effect of the surface charge is the condensation[83] of counter-ion species in non-stoichiometric quantities at this hydrated interfacial layer with the concentration of counter-ions being stabilized at orders of magnitude higher concentrations than what is seen in bulk solution[84]. It is postulated that the electron-dense amorphous layer on the surface of hydrated hydroxyapatite could be highly structured electrostatically[80,81]. The electron-lucent 2 nm width between adjacent crystallite surfaces can accommodate as few as five water molecules spanning the gap[85]. Ionic crowding from the hydrated non-stoichiometric calcium–phosphate layer, when coupled

with confinement, would result in very poor permeability for circulating metabolites into these regions. Investigation of these hydrated mineral interfaces in vitro suggest that only very small metabolic products such as citrate[86], lactate and carbonates[87] might exist as inclusions in between these mineral facets[81], potentially responsible for the spacing of stacked plate-like nanocrystalline morphology often observed[81,88], perhaps occurring through chelation effects. This niche is thus unlikely to harbour the palaeometabolome, attributable to a size exclusion limit that is far smaller than most metabolites detected in this study.

Extant and fossil samples and palaeosols

The bones of two widely used inbred strains of laboratory mouse developed by the Jackson Laboratory were used in this study that were maintained under standard conditions; a constant temperature of 24 °C with a 12 h:12 h light–dark cycle, and food and water ad libitum. They include five female and five male genetically heterogeneous mice (UM-HET3) fed an OpenStandard Diet With 15 kcal% Fat (D11112201, Research Diets) and five male mice from a highly inbred strain (C57BL/6J) fed a standard rodent chow (5053, PicoLab Rodent Diet 20, LabDiet). Concerning bone formation research unrelated to the metabolomics pilot study, the mice were euthanized at six weeks of age, and femurs were dissected (the Institutional Animal Care and Use Committee of New York University approved the animal experiment protocols). Residual soft tissues were carefully removed from the bones with forceps and a surgical scalpel. The metaphyseal ends of the femurs were removed, cutting to the ends of the marrow cavity. The bone marrow was flushed with sterilized cold 1× PBS using a 23-gauge needle syringe until the bone appeared pale. The bones were washed with 1× PBS to eliminate residual soft tissues around the bones. Finally, each bone was weighed using an OHAUS 124/E analytical balance (OHAUS Corporation) to an accuracy of 0.0001 g. Because free water represents less than 6% of the mass of fresh bone[89], which the fossils lack, from extant bones weighing approximately 20 mg, 1 mg was removed from the recorded bone mass in (Supplementary Table 1).

Fossil rodent bones curated at the National Museum of Natural History (NMNH), Paris, France, derive from the palaeontological site of Olduvai Gorge, Tanzania[90], excavated by L. S. B. Leakey in 1960 from Bed I (Table 1). Specimens were acquired by wet and dry sieving, and no specimens have since been touched by hands or been chemically treated. The Olduvai Gorge Bed II fossil was attributed to *K. majus* by G. H. R. von Koenigswald after it was given to him by Leakey in 1954, and is curated at the Senckenberg Research Institute and Natural History Museum, Frankfurt, Germany. The Chiwondo Beds fossil was collected by T.G.B., F.S., O.K. and O.S. in 2000 and curated by the Cultural and Museum Centre Karonga (CMCK), Malawi, and that from Makapansgat was collected by T.G.B. and F.S. in 1982 and curated in the Hard Tissue Research Unit of TGB, New York, USA.

Extant specimens for comparison with the Olduvai Gorge rodents were obtained by C.D. from the Olduvai Gorge vicinity and curated at the NMNH, Paris, France. Extant comparisons for the Chiwondo Beds and Makapansgat fossils were recovered from the skeletons of animals that had lived in Malawi and curated at the CMCK Karonga, Malawi.

Olduvai Gorge palaeosols were obtained by G.M.A. and curated at Rutgers, the State University of New Jersey, USA. Geographical location of collecting sites was determined by GPS and stratigraphic position by geological mapping. Age of stratigraphy was determined by ^{39}Ar–^{40}Ar dating. Samples were collected from measured sections at least 1 m into the exposed face and 1 m down from the top, using a metal spatula. The Chiwondo Beds palaeosol was collected by F.S. at the collecting site of the fossil HCRP-RC-11 883 (Table 1), and that of Makapansgat was collected by T.G.B. and F.S. was taken from the TF12 Lime Dumps breccia several centimetres away from the fossil.

All fossil and extant mineralized tissues and palaeosols were weighed as described for the extant samples.

Histology and imaging

Each fossil bone and corresponding palaeosol was divided into one fraction to obtain ~100 µm-thick histological sections and a fraction for subjecting to the metabolite extraction protocol. Specimens for histology were subject to graded ethanol substitution, infiltrated with methylmethacrylate monomer (Fisher) and polymerized by exposure to ultraviolet light. The polymerized blocks were ground to a uniform 1,200 grit finish using a Buehler Metaserv 250 Grinder-Polisher (Buehler). The ground surface was mounted to an EXAKT methylmethacrylate histology slide (EXAKT Technologies) with cyanoacrylate adhesive, sawn through with the Exakt 300 CP Band System, and ground to about 110 µm thickness with the Exakt 400CS Grinding System. The sections (and adjacent blocks) were then polished using diamond suspension on the Buehler Metaserv to a 1 µm surface finish and approximately 100 µm final section thickness.

Histological sections were imaged by polarized light microscopy using a Leica DMRX/E Universal Microscope or Leica DM5000 B (Leica Microsystems) using Leica PL Apo 20/0.6 or HC PL Fluotar 20/0.5 objective lenses, respectively, to observe the putative presence of collagen birefringence[91].

Sections were then uniformly coated with 10 nm of carbon using a Safematic CCU-010 coating unit (Zizers) and imaged by a Zeiss Gemini 300 field emission scanning electron microscope (FE-SEM; Zeiss), in backscattered electron imaging mode operated at 10 kV and a 60 µm aperture high current setting (~400 pA) beam conditions, and at an 8.5 mm working distance and 97.66 nm per pixel resolution. EDS data were collected using a Bruker Quantax 200 XFlash 6160 EDS detector and Esprit v.2.6 software (Bruker) for determining the normalized mass concentration of elements within 100 µm field widths yielding x-ray signals generated from a beam radius of 1 µm with a 1.7 µm interaction depth; the normalized mass concentration of carbon was adjusted in Esprit software to compensate for the 10 nm carbon coating thickness. We used the P/B-ZAF standardless analysis quantification model in interactive mode to validate each element peak. To evaluate sample integrity, we were explicitly interested in recording the Ca/P ratio for fossil and extant bones and comparing them to the chemistries of the palaeosols.

Extraction protocol

Each extant and fossil bone sample and palaeosol sample and diet samples of the two laboratory mouse strains was placed into their own 1.5 ml Eppendorf vial containing 2 µl of 4% formic acid (147932500, Acros Organics, Thermo Scientific) per 1 mg of hard tissue prepared in sterilized molecular biology grade water (46-000-CM, Corning, Mediatech). Formic acid was used as the demineralizing agent for all bone samples because at low concentrations it best preserves collagen over other common demineralizing agents[92] and thus, we presume, other biomolecules, and also because sample delivery to the mass spectrometer utilizes a weak formic acid solution (see below), therefore maintaining a consistent matrix from preparation of the sample through to mass spectrometry metabolomics analysis. Palaeosol and diet samples were prepared in exactly the same way as the bone samples.

The vials were left overnight at 4 °C on a shaker, and extracts were collected, transferred to a new 1.5 ml vial, and stored at −80 °C. The remaining un-demineralized sample was treated with fresh extraction solvent and kept overnight at 4 °C on the shaker. The extracts were then transferred to the vials that contained the first extracts collected previously. In total, extracts were collected from three such treatments. The extracts were kept at −80 °C until preparation for metabolomics and proteomics analysis.

Extracts collected from all mineralized tissue samples were transparent and slightly viscous. After the three treatments, any 'solid' non-solubilized bone collagen anlage was removed from the vial of each specimen.

One experiment deviated from the above protocol to test the effect of enzymatic digestion of bone before the extraction protocol. This experiment treated long bone fragments from two C57BL-6J mice with a ~1% Tergazyme solution (Alconox) at 37 °C for 48 h. These fragments were then rinsed in running tap water for 30 min and then subjected to the extraction protocol with the non-enzymatically treated bone fragments from two other C57BL-6J mice, as described above.

Metabolomics analysis

Samples were allowed to thaw, upon which methanol (LC–MS Grade) was added to each sample, giving final concentrations of 75% (v/v) methanol (HPLC grade, Fisher Scientific) in the fossil and palaeosol sample mixtures and 62.5% (v/v) methanol in the laboratory mouse and extant bone sample mixture. The protein content in each mineralized tissue sample was precipitated overnight by −80 °C freezer storage. On the next day, each sample was vortex-mixed and centrifuged for 30 min at 4 °C and 14,000 rpm. The methanolic supernatant layers containing metabolites were transferred to clean Eppendorf vials and were evaporated to near dryness under vacuum using a SpeedVac vacuum concentrator (Thermo Fisher Scientific). Each sample was reconstituted with 10 µl of 0.1% (v/v) formic acid in water, vortex-mixed, and transferred into liquid chromatography–tandem mass spectrometry (LC–MS/MS) vials for analysis. Nano-LC–MS/MS was performed using a QExactive HF-X mass spectrometer coupled directly to a Vanquish UHPLC system (Thermo Scientific). One-microlitre aliquots of each sample were injected onto a Hypersil Gold C18 100 ×1 mm column (Thermo Scientific), which was maintained at a constant temperature of 50 °C, equilibrated with mobile phase A containing 0.1% (v/v) formic acid in HPLC grade water. Metabolites were eluted with a 0–60% methanol containing 0.1% (v/v) formic acid (mobile phase B) with a flow rate of 50 µl min^{-1} over 22 min, followed by 60–100% B over 3 min, then back to 0% B at 27 min. The sample volume injected was 1 µl. This sample preparation method was adapted from ref. 93.

Each sample was analysed twice, and the mass spectrometer was operated in positive and negative ion modes using a data-dependent acquisition mode. Up to five most abundant precursors from the survey scans acquired at a resolution of 120,000 over a scan range of m/z 200–2,000 were selected with an isolation window of 1.7 Th (a unit of mass-to-charge ratio) and fragmented by higher-energy collisional dissociation with a normalized collision energy setting of 30. The maximum ion injection time for the survey and MS/MS scans was 75 ms, and the ion target values for MS and MS/MS scans were set at 3×10^6 and 1×10^5, respectively.

Raw mass spectrometry data from positive and negative ion mode analyses were subjected to a metabolomics database search using Compound Discoverer 3.1 (Thermo Scientific). All detected metabolites were annotated to include compound name, formula, molecular mass, minimum retention time, maximum area under the detection peak and known identifier (ID) (Supplementary Table 1). Each metabolite ID was interrogated in a quality control step by searching Chemical Abstracts Service (CAS; https://www.cas.org/cas-data/cas-registry), PubChem (https://pubchem.ncbi.nlm.nih.gov) and ChemSpider (https://www.chemspider.com) online databases, ensuring that formula, mass and compound name matched. In all supplementary tables, tabs labelled 'Total IDs' all survived quality control and have at least a formula and compound name.

Proteomics analysis

Following the transfer of the metabolite supernatant of four Olduvai Gorge fossil rodents (M-D, Sm, Gg and Xi), the protein precipitate after methanolic extraction was subjected to solubilization in 8 M urea in Tris pH 7.5. Protease inhibitors (Mini, Roche) were added to each sample before the proteins were reduced and alkylation was achieved. Next, the concentration of the urea was adjusted to 1 M urea and samples were supplemented with 12.5 ng ml^{-1} trypsin solution (Trypsin Gold, Mass Spectrometry Grade, Promega) in 50 mM NH_4HCO_3 and incubated at 37 °C overnight. Peptides were acidified to 1% formic acid (w/v), and centrifuged at 14,000*g* to remove debris. Desalting of peptides was done using hand-packed SPE Empore C18 Extraction Disks (also known as Stage Tips, 3M)[94]. Samples were concentrated to a small volume by vacuum centrifugation and peptides reconstituted in 2% acetonitrile/4% formic acid. Nano liquid chromatography coupled to tandem mass spectrometry (nano-LC–MS/MS) was carried out as described previously[95].

The mass spectra files were subjected to MaxQuant proteomics data analysis workflow (v.2.5.1.0) with the Andromeda search engine[96]. Raw mass spectrometer files were used to extract peak lists, which were searched with the Andromeda search engine against mouse proteomes, and a file containing contaminants such as human keratins. Trypsin specificity with 2 missed cleavages with the minimum required peptide length was set to seven amino acids. *N*-acetylation of protein N termini, oxidation of methionines, deamidation of asparagine and glutamine and pyroglutamate conversion of glutamine and glutamic acid and finally, hydroxylation of proline residues were set as variable modifications. To identify peptides, we used UniProt rodent databases (mouse: 21,985, rat: 22,825, Chinese hamster: 23,883, guinea pig: 18,246 protein sequence entries, downloaded 4 October 2022). For the initial main search, parent peptide masses were allowed a mass deviation of 20 ppm. Peptide spectral matches and protein identifications were filtered using a target-decoy approach at a false discovery rate of 1%. In order to generate spectral libraries with the modifications we set out, we first used data-dependent-acquisition (DDA) mass spectrometry as described[95] and obtained evidence and MS/MS text files. Next, samples were analysed with Data-Independent-Acquisition (DIA)[97], and utilizing MaxDIA embedded in MaxQuant software, the DIA files were searched using the spectral libraries obtained with the DDA experiment.

Analysis of endogenous metabolites

The IPA (QIAGEN) program was used to analyse mammalian endogenous metabolites and their respective top canonical pathways, biological functions and gene networks. Default analysis settings were used with searchable databases including mouse, rat, and human, which constitute all currently published conserved mammalian core metabolomic processes.

These pathways, biological functions and networks do not represent an instantaneous metabolome, but one that is summed over the period of time mineralized tissue was forming. The header of each of fossil and extant metabolite ID table (Supplementary Tables 4a–11a) gives the number of metabolite annotations from *N* number of features. The number of annotations is a fraction of the combined endogenous (Supplementary Tables 4a–11b) and exogenous (Supplementary Tables 4c–11c) metabolite numbers because of restrictions IPA places on the Ingenuity Knowledge Base (https://qiagen.my.salesforce-sites.com/KnowledgeBase?id=kA41i000000L5sBCAS). The largest database of its kind, metabolites are rigorously vetted in quality control for their probability of describing the biological functions given.

IPA discriminates non-mammalian exogenous from endogenous metabolites, but they are not analysed. There does not presently exist a database against which exogenous metabolites may be queried for their ecological inferences, thus, by this communication we originate one. The procedure for classifying exogenous metabolites into major categories and selecting the likely candidate organisms from which the metabolites were derived and used to document environmental characteristics, is described below.

Analysis of exogenous metabolites

Exogenous metabolites identified in the IPA analyses of each fossil sample were assigned using a template of 15 categories (Supplementary Tables 4k–8k, 10k and 11k), which include: (1) geology; (2) fire; (3) bacteria; (4) aquatic; (5) fungi; (6) non-flowering plant; (7) flowering

monocotyledons; (8) flowering magnoliids; (9) flowering eudicotyledons; (10) plant wound healing; (11) parasite; (12) insect; (13) numerous organisms; (14) anomalies; and (15) unknown. Of the eight fossil samples reported in this study, no specimen exhibited small molecules associated with geophagy, but in observations of other fossil bone metabolomes not reported here we have, so the geology category is maintained in the template.

In most cases, candidate sources of metabolites were assessed from the Taxonomy section of PubChem. If this was unrewarding, we attempted internet searches for information. Typically, if the list of metabolite sources occupied 15 of this section's pages (containing 5 metabolite sources per page) or less, each source was considered for its likelihood of expression in the fossil sample. For instance, if bacteria were the main entries, and no plant source suited the regional geographic context (that is, eastern, central, or southern Africa), then bacteria were likely to be the source. Plant sources were searched in the Royal Botanic Gardens online database (https://powo.science.kew.org) and were considered likely if their geographic distribution included either eastern Africa for Olduvai Gorge, central Africa for the Chiwondo Beds, or southern Africa for Makapansgat. Often, plant species associated with a metabolite are not represented in the geographic region of interest; this simply reflects the capricious search for factors in medicinal plants described in the main text. However, candidate species within genera are commonly observed to share metabolomes. For instance, the metabolite 4-methylbenzoic acid (PubChem ID 7470) is found in *Aloe vera*, yet it is also a metabolite of *Aloe africana*, *Aloe spicata* and *Aloe ferox*, which also happened to be assayed. Thus, candidate species are typically used in the associations between metabolites and plant species. Rarely we chose regional candidate plants in the same family.

Anomalies of category 14 are attributable to contaminants. They comprise drug categories (for example, antimalarials), sunscreen and lotions, and insect repellents, all of which we surmise are at researchers' fingertips in African collecting sites and palaeontological laboratories. They also include adhesives, silicone-based products, and resins common in these laboratories.

A first attempt to acquire plant habitat information on soil characteristics, minimum and maximum rainfall (mm year^{-1}), minimum and maximum temperature (°C), open versus closed conditions, and elevation (m) was then made by searching the Useful Tropical Plants online database (https://tropical.theferns.info). Additional environmental information was also acquired from Internet searches, and websites were recorded.

We undertook the environmental reconstruction as detailed above for *K. majus* from Olduvai Gorge Bed II (Supplementary Table 9c). However, additionally, we further pruned the list of metabolites to those that supported isotopic evidence attributed to this species and those plants otherwise known to be opportunistically favoured by extant pigs (Supplementary Table 9d).

Statistical tests and data visualization

To investigate the variance in metabolomic signatures across fossil, soil, and modern biological samples, we applied a multi-method statistical framework using Python v.3.10.12. Our analysis focused on the 100 most variable metabolites, defined by highest variance in intensity values across the combined dataset (Supplementary Table 14a). We performed unsupervised and supervised techniques including PCA, hierarchical clustering, ANOVA, Kruskal–Wallis tests and PLS-DA to identify and visualize biologically meaningful separation among sample groups. Statistical tests such as ANOVA and Kruskal–Wallis were performed using the SciPy library[98]. Visualizations such as PCA scatter plots and hierarchical clustering heat maps were created using the Seaborn package[99]. PLS-DA was performed using the PLSRegression module in Scikit-learn, adapted for classification by labelling categorical outcomes numerically[100].

Data preparation. Raw metabolite abundance data were pivoted to form a matrix of samples (rows) by metabolite features (columns). Each metabolite's variance was calculated across all samples. The top 100 most variable metabolites were selected for downstream analyses. Group labels (for example, Fossil, Soil or Modern) were assigned per sample.

Principal component analysis. We standardized the data using StandardScaler function from Scikit-learn[100] and conducted PCA on the top 100 metabolites. The first two principal components (PC1 and PC2) explained the majority of variance. PCA plots revealed clear grouping of samples by biological origin, with fossil samples clustering apart from soils and modern controls.

Hierarchical clustering. A hierarchical clustering heat map of *z*-score-normalized data (top 100 metabolites) was generated using average linkage and Euclidean distance. Clustered groupings visually confirmed PCA results, showing distinct metabolic signatures for each sample type.

Univariate statistical testing. One-way ANOVA was used to test for significant differences in metabolite abundance across sample categories. We identified several metabolites with P values < 0.01, including methyl acetoacetate, kojic acid and myristohydroxamic acid. To validate results under non-parametric conditions, we performed Kruskal–Wallis tests, which confirmed overlapping top hits.

PLS-DA. PLS-DA was implemented using Scikit-learn's PLSRegression, followed by supervised classification of group categories. The model's discriminative power was visualized in 2D space and assessed via VIP scores. Clear separation between categories was observed in PLS1 versus PLS2 space. VIP scores were calculated to identify metabolites contributing most to class discrimination. Many top VIP hits overlapped with those identified in ANOVA and PCA loadings.

Reporting summary

Further information on research design is available in the Nature Portfolio Reporting Summary linked to this article.

Data availability

The raw mass spectrometry metabolomics data generated during this study are available at MassIVE (UCSD) (https://massive.ucsd.edu/ProteoSAFe/static/massive.jsp) under the deposition number MSV000097146. Proteomics LC–MS data (proteomics raw mass spectrometry data, peak lists and results) that support the findings of this study are deposited to the ProteomeXchange Consortium via the MassIVE partner repository and can be retrieved with the accession code MSV000097173 and with the dataset identifier PXD061016.

61. Boyde, A. & Jones, S. J. Aspects of anatomy and development of bone: the nm, μm and mm hierarchy. *Adv. Organ Biol.* **5**, 3–44 (1998).
62. Buss, D. J., Kröger, R., McKee, M. D. & Reznikov, N. Hierarchical organization of bone in three dimensions: a twist of twists. *J. Struct. Biol. X.* **30** 6, 100057 (2022).
63. Grandfield, K., Vuong, V. & Schwarcz, H. P. Ultrastructure of bone: hierarchical features from nanometer to micrometer scale revealed in focused ion beam sections in the tem. *Calcif. Tissue Int.* **103**, 606–616 (2018).
64. Bell, L. C. & Mika, H. The pH dependence of the surface concentrations of calcium and phosphorus on hydroxyapatite in aqueous solutions. *J. Soil Sci.* **30**, 247–258 (1979).
65. Bell, L. C., Posner, A. M. & Quirk, J. P. Surface charge characteristics of hydroxyapatite and fluorapatite. *Nature* **239**, 515–517 (1972).
66. Itoh, D., Yoshimoto, N. & Yamamoto, S. Retention mechanism of proteins in hydroxyapatite chromatography – multimodal interaction based protein separations: a model study. *Curr. Protein Pept. Sci.* **20**, 75–81 (2018).
67. Kendall, C., Eriksen, A. M. H., Kontopoulos, I., Collins, M. J. & Turner-Walker, G. Diagenesis of archaeological bone and tooth. *Palaeogeogr. Palaeoclimatol. Palaeoecol.* **491**, 21–37 (2018).
68. Buffrénil, V. D. *Vertebrate Skeletal Histology and Paleohistology* (CRC Press, 2021).
69. Jans, M. M. E. in *Current Developments in Bioerosion* (eds Wisshak, M. & Tapanila, L.) 397–413 (Springer, 2008).

70. Jackes, M., Sherburne, R., Lubell, D., Barker, C. & Wayman, M. Destruction of microstructure in archaeological bone: a case study from Portugal. *Int. J. Osteoarchaeol.* **11**, 415–432 (2001).
71. Turner–Walker, G. & Syversen, U. Quantifying histological changes in archaeological bones using BSE–SEM image analysis. *Archaeometry* **44**, 461–468 (2002).
72. Buss, D. J., Reznikov, N. & McKee, M. D. Crossfibrillar mineral tessellation in normal and *Hyp* mouse bone as revealed by 3D FIB-SEM microscopy. *J. Struct. Biol.* **212**, 107603 (2020).
73. McKee, M. D., Buss, D. J. & Reznikov, N. Mineral tessellation in bone and the stenciling principle for extracellular matrix mineralization. *J. Struct. Biol.* **214**, 107823 (2022).
74. Reznikov, N. et al. Biological stenciling of mineralization in the skeleton: local enzymatic removal of inhibitors in the extracellular matrix. *Bone* **138**, 115447 (2020).
75. Reznikov, N., Bilton, M., Lari, L., Stevens, M. M. & Kroeger, R. Fractal-like hierarchical organization of bone begins at the nanoscale. *Science* **360**, eaao2189 (2018).
76. Bertassoni, L. E. & Swain, M. V. The contribution of proteoglycans to the mechanical behavior of mineralized tissues. *J. Mech. Behav. Biomed. Mater.* **38**, 91–104 (2014).
77. Scott, J. E. Proteoglycan-fibrillar collagen interaction. *Biochem. J* **252**, 313–323 (1988).
78. Fantner, G. E. et al. Sacrificial bonds and hidden length dissipate energy asmineralized fibrils separate during bone fracture. *Nat. Mater.* **4**, 612–615 (2005).
79. Walsh, W. R. & Guzelsu, N. Ion concentration effects on bone streaming potentials and zeta potentials. *Biomaterials* **14**, 331–336 (1993).
80. Wang, Y. et al. Water-mediated structuring of bone apatite. *Nat. Mater.* **12**, 1144–1153 (2013).
81. Duer, M. J. The contribution of solid-state NMR spectroscopy to understanding biomineralization: atomic and molecular structure of bone. *J. Magn. Reson.* **253**, 98–110 (2015).
82. Fullerton, G. D. & Amurao, M. R. Evidence that collagen and tendon have monolayer water coverage in the native state. *Cell Biol. Int.* **30**, 56–65 (2006).
83. Stigter, D. Evaluation of the counterion condensation theory of polyelectrolytes. *Biophys. J.* **69**, 380–388 (1995).
84. Israelachvili, J. N. *Intermolecular and Surface Forces*, 3rd edn (Academic Press, 2015).
85. Urbic, T. Ions increase strength of hydrogen bond in water. *Chem. Phys. Lett.* **610–611**, 159–162 (2014).
86. Jiang, W., Griffanti, G., Tamimi, F., McKee, M. D. & Nazhat, S. N. Multiscale structural evolution of citrate-triggered intrafibrillar and interfibrillar mineralization in dense collagen gels. *J. Struct. Biol.* **212**, 107592 (2020).
87. Li, Y. et al. Metabolic acids impact bone mineral maturation. Preprint at *bioRxiv* https://doi.org/10.1101/2022.09.21.508894 (2022).
88. Hu, Y.-Y., Rawal, A. & Schmidt-Rohr, K. Strongly bound citrate stabilizes the apatite nanocrystals in bone. *Proc. Natl Acad. Sci. USA* **107**, 22425–22429 (2010).
89. Abbasi-Rad, S. & Rad, H. S. Quantification of human cortical bone bound and free water in vivo with ultrashort echo tiome MR imaging: a model-based aproach. *Radiology* **283**, 862–872 (2017).
90. Leakey, L. S. B. *Olduvai Gorge 1951–61: Volume 1, A Preliminary Report on the Geology and Fauna* (Cambridge Univ. Press, 1965).
91. Bromage, T. G. et al. Circularly polarized light standards for investigations of collagen fiber orientation in bone. *Anat. Rec.* **274B**, 157–168 (2003).
92. Pang, S. et al. Comparison of different protocols for demineralization of cortical bone. *Sci. Rep.* **11**, 7012 (2021).
93. Deng, J., Zhang, G. & Neubert, T. A. Metabolomic analysis of glioma cells using nanoflow liquid chromatography–tandem mass spectrometry. *Methods Mol. Biol.* **1741**, 125–134 (2018).
94. Rappsilber, J., Mann, M. & Ishihama, Y. Protocol for micro-purification, enrichment, pre-fractionation and storage of peptides for proteomics using StageTips. *Nat. Protoc.* **2**, 1896–1906 (2007).
95. Xu, Y. et al. Cardiolipin remodeling enables protein crowding in the inner mitochondrial membrane. *EMBO J.* **40**, e108428 (2021).
96. Tyanova, S., Temu, T. & Cox, J. The MaxQuant computational platform for mass spectrometry based shotgun proteomics. *Nat. Protoc.* **11**, 2301–2319 (2016).
97. Sinitcyn, P. et al. MaxDIA enables library-based and library-free data-independent acquisition proteomics. *Nat. Biotechnol.* **39**, 1563–1573 (2021).
98. Virtanen, P. et al. SciPy 1.0: fundamental algorithms for scientific computing in Python. *Nat. Methods* **17**, 261–272 (2020).
99. Waskom, M. L. Seaborn: statistical data visualization. *J. Open Source Softw.* https://doi.org/10.21105/joss.03021 (2021).
100. Pedregosa, F. et al. Scikit-learn: machine learning in Python. *J. Mach. Learn. Res.* **12**, 2825–2830 (2011).

Acknowledgements Funding for this project was provided by The Leakey Foundation (grant number Spring202310420) to T.G.B. We thank all institutions, which provided and supported sampling: the CMCK Karonga, Malawi, NMHN Paris, France, and the Senckenberg Research Institute and the Natural History Museum Frankfurt, Germany. We express our gratitude to the Werner Reimers Foundation in Bad Homburg, Germany, which provides the Gustav Heinrich Ralph von Koenigswald collection as a permanent loan for scientific research to the Senckenberg Research Institute and Natural History Museum Frankfurt. Thanks go to the New York University Grossman School of Medicine's Applied Bioinformatics Laboratories for access to QIAGEN IPA. The Zeiss Gemini 300 FE-SEM used for evaluating bone microanatomy was provided courtesy of the National Institutes of Health S10 Shared Instrumentation Program, grant number 1S10OD026989-01; mass spectrometry instrumentation, National Institutes of Health grant numbers S10 OD023659 and S10 RR027990. We thank P. Ausili and L. Kaleel for assistance with metabolite annotations and data organization. N.R. and M.D.M. are members of the Fonds de Recherche du Québec–Santé (FRQS) Centre for Structural Biology Research at McGill University, and the FRQS Network for Intersectorial Research in Sustainable Oral and Bone Health. M.D.M. is the Canada Research Chair in Biomineralisation, and N.R. is a William Dawson Scholar at McGill University. A.S. is supported by the French government in the framework of the University of Bordeaux's IdEx 'Investments for the Future' programme/GPR 'Human Past'. This project is an outcome of the 2010 Max Planck Research Award to T.G.B., endowed by the German Federal Ministry of Education and Research to the Max Planck Society and the Alexander von Humboldt Foundation in respect of the Hard Tissue Research Program in Human Paleobiomics.

Author contributions T.G.B. conceived the study and led the work. C.D., J.K., O.K., F.S. and O.S. prepared and provided fossil samples and extant representatives of African species. G.M.A. and C.D. provided palaeosols. S.Y. and S.B.P. prepared and provided the extant laboratory mouse material, A.S. provided likelihoods of plant resources based on isotopic evidence. B.H. undertook the histology and light and electron microscopy. S.R. produced the fossil bone extracts. T.A.N., C.L.D.J. and H.E.-B. performed the metabolomics and proteomics and their relevant bioinformatics. M.D.M., N.R., D.J.B. and E.I. elaborated the interpretation of the bone ultrastructural metabolite niches. T.G.B. and S.R. annotated the metabolite lists from online databases, and T.G.B. interpreted the metabolic and ecological profiles and wrote the manuscript, with valuable contributions from all co-authors.

Competing interests The authors declare no competing interests.

Additional information

Supplementary information The online version contains supplementary material available at https://doi.org/10.1038/s41586-025-09843-w.

Correspondence and requests for materials should be addressed to Timothy G. Bromage.

Peer review information *Nature* thanks Yolanda Fernández-Jalvo, Jasmina Wiemann and the other, anonymous, reviewer(s) for their contribution to the peer review of this work.

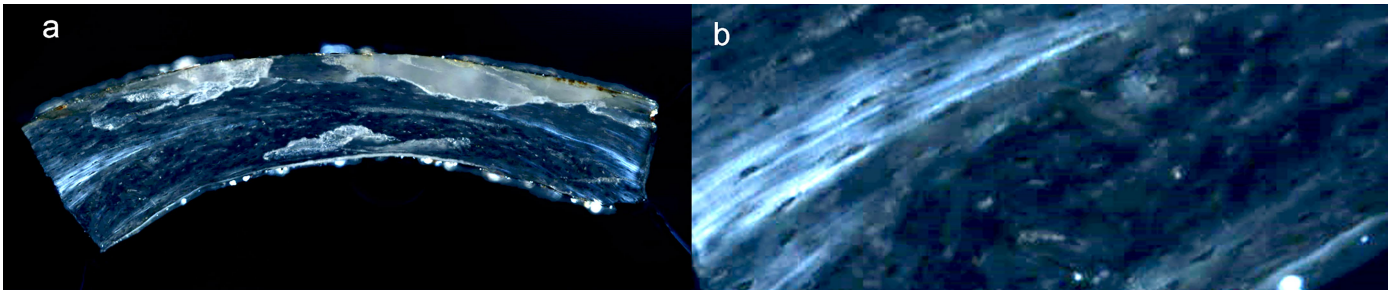

Extended Data Fig. 1 | Polarised light images of specimen M-D. *Mus* sp. or *Dendromus* sp., Bed I, Level FLKN1 M3. a. Birefringent brightness at top and bottom is attributed to heavily crystalised bone domains, while the central curvilinear arc of brightness is attributed to collagen. FW = 1.547 mm; b) Detail of bright bone lamellae and osteocyte lacunae interspersed among them. FW = 0.324 mm.

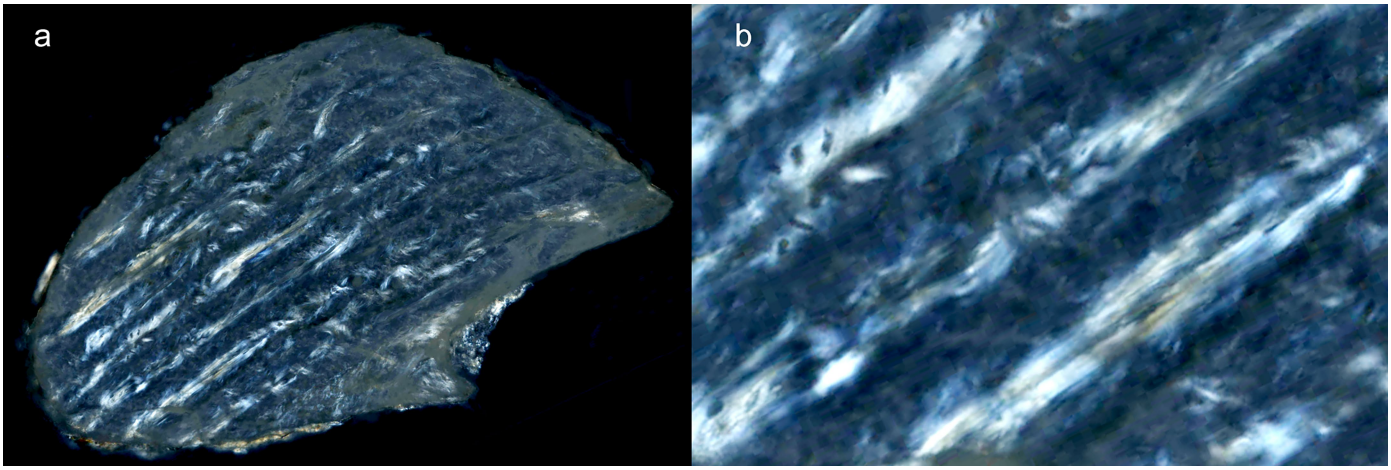

Extended Data Fig. 2 | Polarised light image of specimen Sm. *Saccostomus* cf. *mearnsi*, Bed I, Level FLKN1. a. Birefringent brightness is attributed to collagen. FW = 1.343 mm; b) Detail of bright domains and osteocyte lacunae interspersed among them. FW = 0.324 mm.

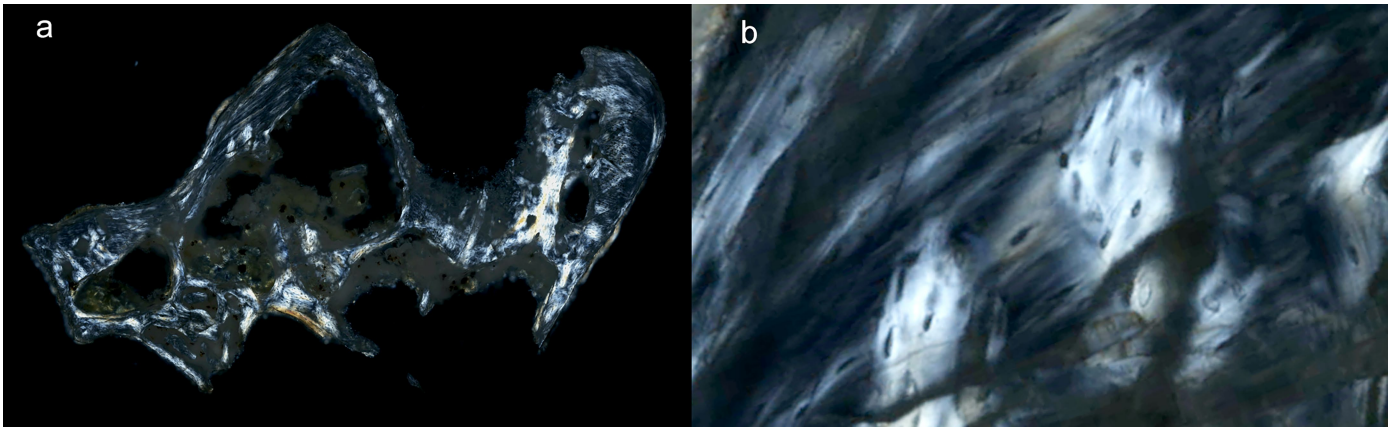

Extended Data Fig. 3 | Polarised light image of specimen Gg. *Gerbilliscus gentryi*, Bed I, Level FLKN1 M1. a. Birefringent brightness is attributed to collagen. FW = 3.922 mm; b) Detail of bright domains and osteocyte lacunae interspersed among them. FW = 0.324 mm.

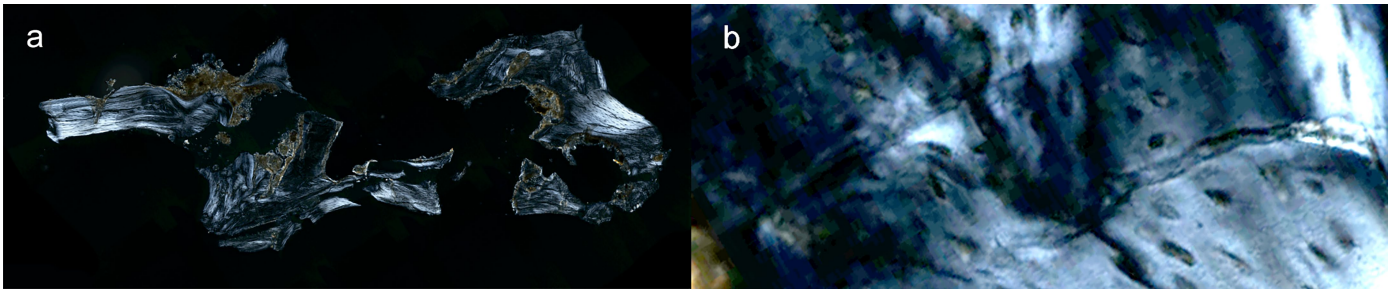

Extended Data Fig. 4 | Polarised light image of specimen Gi. *Gerbilliscus* sp. indet, Bed I, Level DK. a. Birefringent brightness is attributed to collagen. FW = 4.506 mm; b) Detail of bright domains and osteocyte lacunae interspersed among them. FW = 0.324 mm.

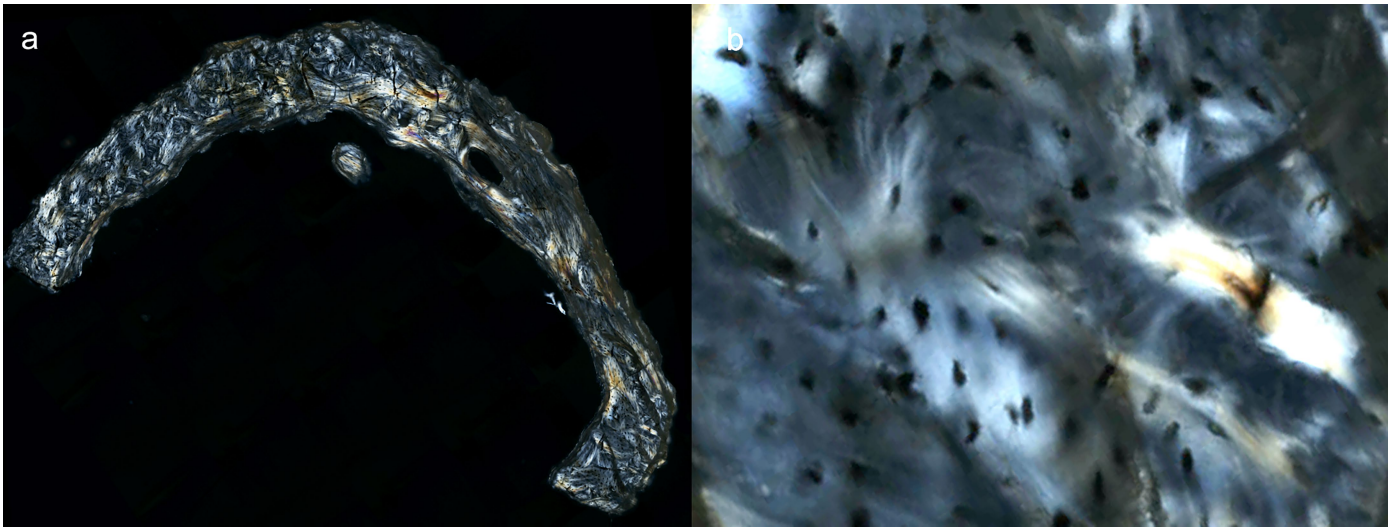

Extended Data Fig. 5 | Polarised light image of specimen Xi. *Xerus* cf. *inauris*, Bed I, Level FLKN1 M3. a. Birefringent brightness is attributed to collagen. FW = 4.434 mm; b) Detail of bright domains and osteocyte lacunae interspersed among them. FW = 0.324 mm.

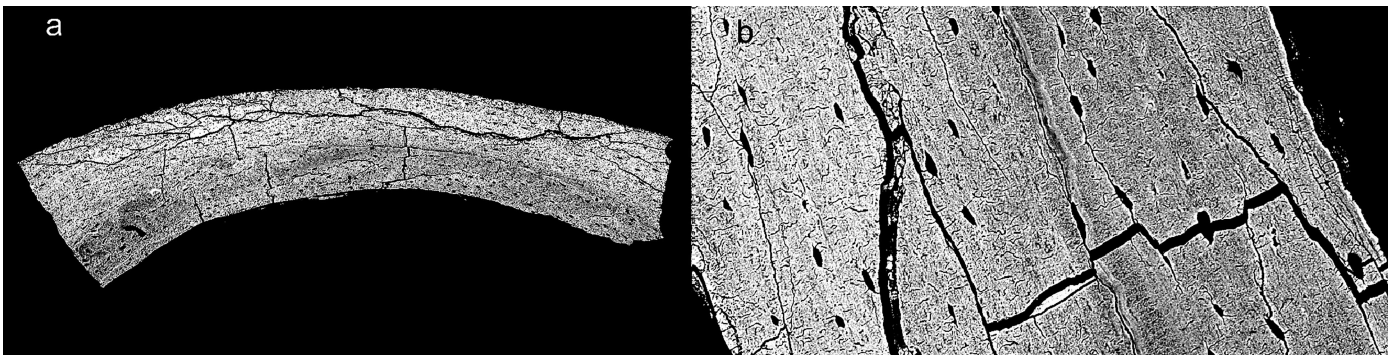

Extended Data Fig. 6 | BSE-SEM image of specimen M-D. *Mus* sp. or *Dendromus* sp., Bed I, Level FLKN1 M3. a. Macroscopic view of the bone fragment. FW = 1.515 mm; b. Detail of bone and osteocyte lacunae and their associated canaliculi. Large cracks are due to diagenesis or preparation. FW = 0.25 mm.

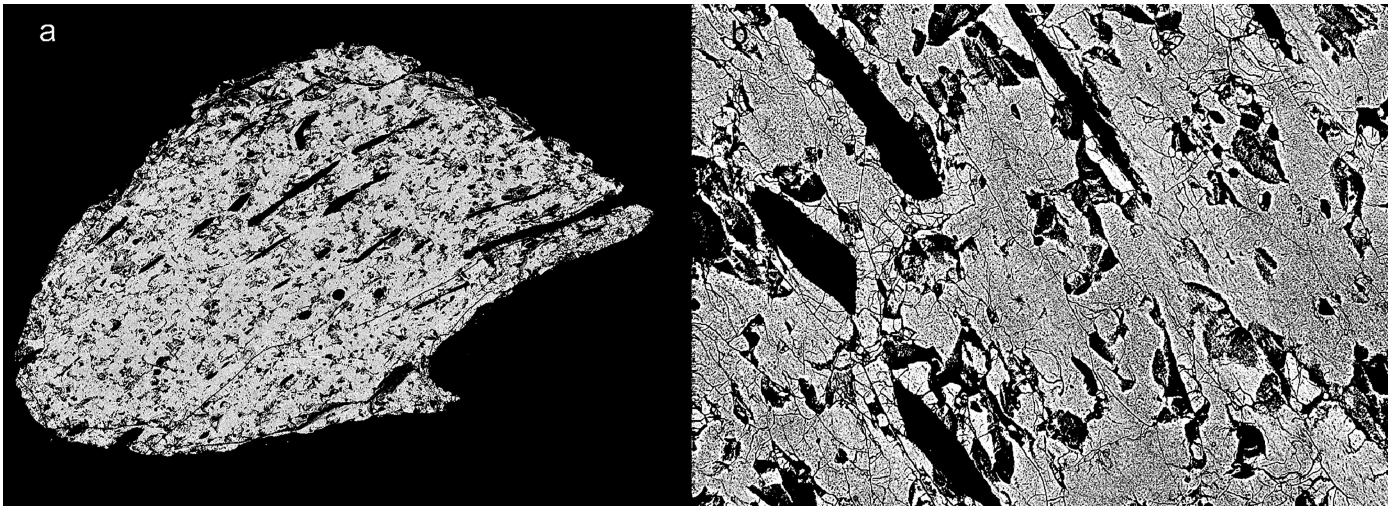

Extended Data Fig. 7 | BSE-SEM image of specimen Sm. *Saccostomus* cf. *mearnsi*, Bed I, Level FLKN1. a. Macroscopic view of the bone fragment. FW = 1.329 mm; b. Detail of bone illustrating diagenetically disorganized bony structure but preserving some vascular canals and osteocyte lacunae. FW = 0.25 mm.

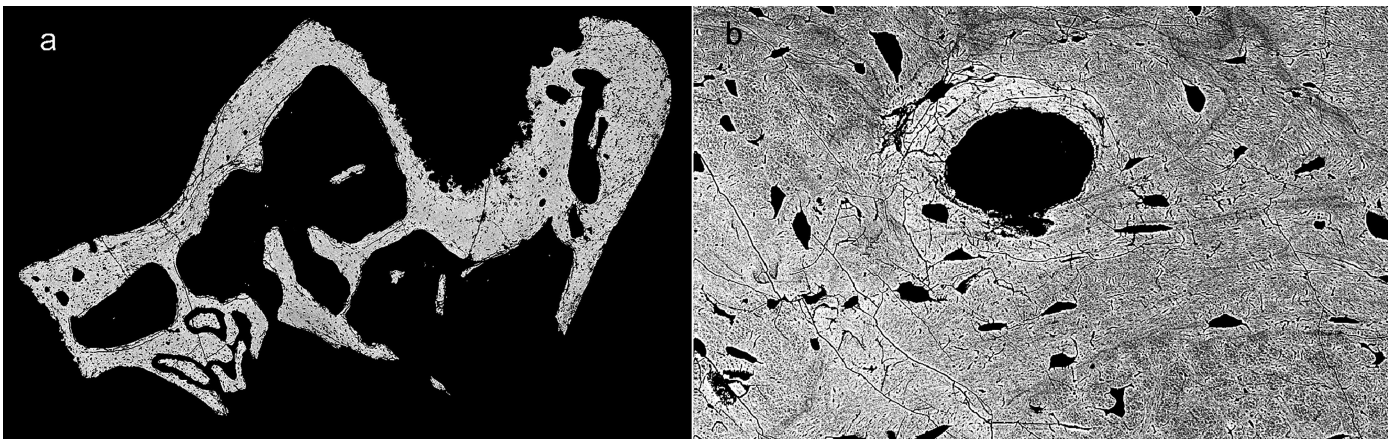

Extended Data Fig. 8 | BSE-SEM image of specimen Gg. *Gerbilliscus gentryi*, Bed I, Level FLKN1 M1. a. Macroscopic view of the bone fragment. FW = 3.726 mm; b. Detail of bone illustrating a vascular canal, mineralization density variation, and osteocyte lacunae and their associated canaliculi. FW = 0.25 mm.

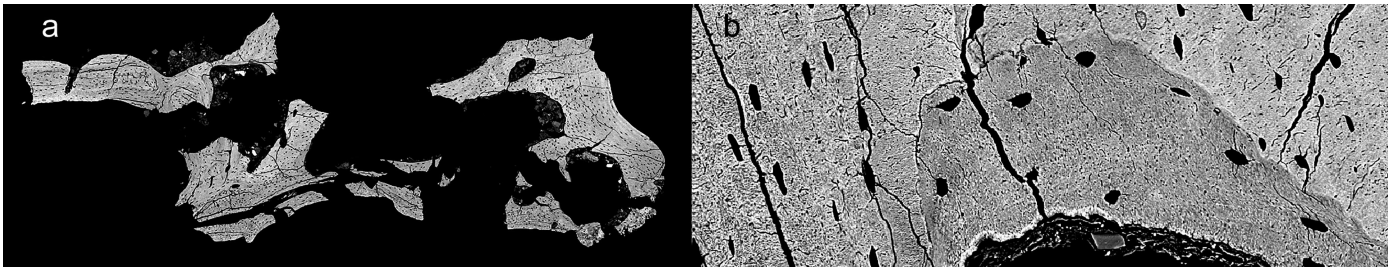

Extended Data Fig. 9 | BSE-SEM image of specimen Gi. *Gerbilliscus* sp. indet, Bed I, Level DK. a. Macroscopic view of the bone fragment. FW = 4.261 mm; b. Detail of bone illustrating a vascular canal (bottom), mineralization density variation, and osteocyte lacunae and their associated canaliculi. Large cracks are due to diagenesis or preparation. FW = 0.25 mm.

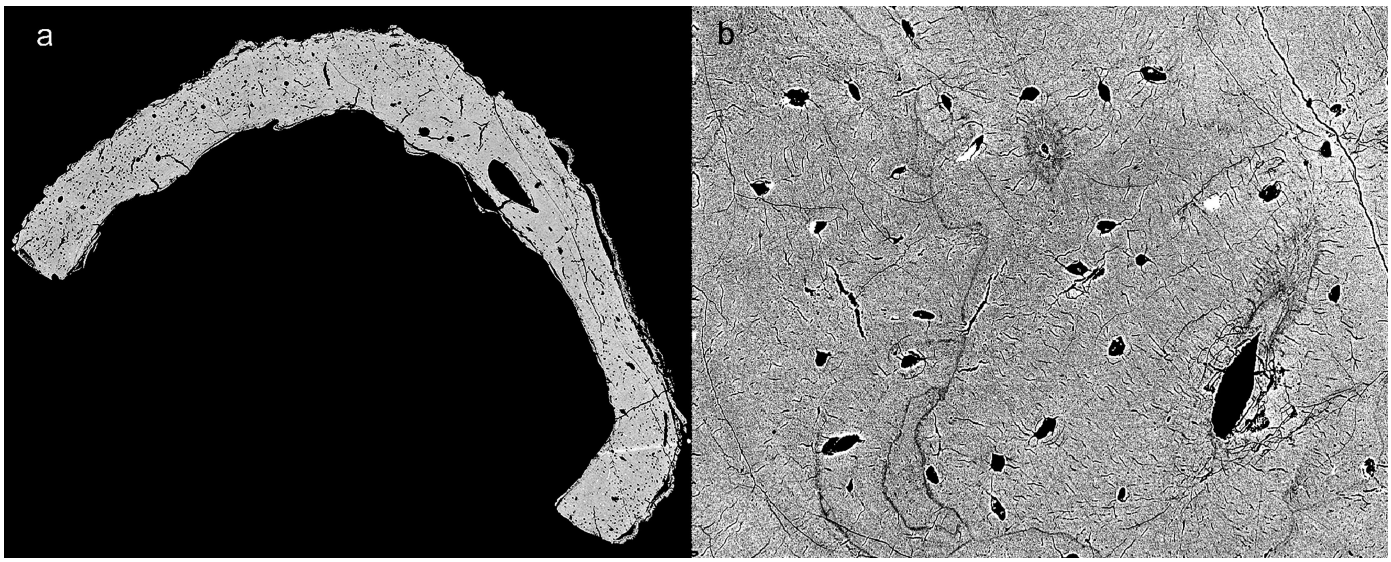

Extended Data Fig. 10 | BSE-SEM image of specimen Xi, *Xerus* cf. *inauris*, Bed I, Level FLKN1 M3. a. Macroscopic view of the bone fragment. FW = 4.211 mm; b. Detail of bone illustrating a vascular canal, mineralization density variation, and osteocyte lacunae and their associated canaliculi. FW = 0.25 mm.

nature portfolio

Corresponding author(s): Timothy G. Bromage

Last updated by author(s): October 20, 2025

Reporting Summary

Nature Portfolio wishes to improve the reproducibility of the work that we publish. This form provides structure for consistency and transparency in reporting. For further information on Nature Portfolio policies, see our Editorial Policies and the Editorial Policy Checklist.

Statistics

For all statistical analyses, confirm that the following items are present in the figure legend, table legend, main text, or Methods section.

n/a	Confirmed
☐	☒ The exact sample size (*n*) for each experimental group/condition, given as a discrete number and unit of measurement
☐	☒ A statement on whether measurements were taken from distinct samples or whether the same sample was measured repeatedly
☐	☒ The statistical test(s) used AND whether they are one- or two-sided *Only common tests should be described solely by name; describe more complex techniques in the Methods section.*
☒	☐ A description of all covariates tested
☐	☒ A description of any assumptions or corrections, such as tests of normality and adjustment for multiple comparisons
☐	☒ A full description of the statistical parameters including central tendency (e.g. means) or other basic estimates (e.g. regression coefficient) AND variation (e.g. standard deviation) or associated estimates of uncertainty (e.g. confidence intervals)
☐	☒ For null hypothesis testing, the test statistic (e.g. *F*, *t*, *r*) with confidence intervals, effect sizes, degrees of freedom and *P* value noted *Give P values as exact values whenever suitable.*
☒	☐ For Bayesian analysis, information on the choice of priors and Markov chain Monte Carlo settings
☐	☒ For hierarchical and complex designs, identification of the appropriate level for tests and full reporting of outcomes
☐	☒ Estimates of effect sizes (e.g. Cohen's *d*, Pearson's *r*), indicating how they were calculated

Our web collection on statistics for biologists contains articles on many of the points above.

Software and code

Policy information about availability of computer code

Data collection	No computer code was used
Data analysis	Online commericial software, Ingenuity Pathway Analysis, was used to analyse the metabolome, and proteomics data analysis was performed using MaxQuant (version 2.5.1.0)

For manuscripts utilizing custom algorithms or software that are central to the research but not yet described in published literature, software must be made available to editors and reviewers. We strongly encourage code deposition in a community repository (e.g. GitHub). See the Nature Portfolio guidelines for submitting code & software for further information.

Data

Policy information about availability of data

All manuscripts must include a data availability statement. This statement should provide the following information, where applicable:

- Accession codes, unique identifiers, or web links for publicly available datasets
- A description of any restrictions on data availability
- For clinical datasets or third party data, please ensure that the statement adheres to our policy

The raw mass spectrometry metabolomics data generated during this study are available at MassIVE (UCSD), https://massive.ucsd.edu/ProteoSAFe/static/massive.jsp under the deposition number MSV000097146. Proteomics LC-MS data (proteomics raw mass spectrometry data, peak lists, and results) that support

the findings of this study are deposited to the ProteomeXchange Consortium via the MassIVE partner repository and can be retrieved with the accession code MSV000097173 and with the dataset identifier PXD061016. Protein sequences (FASTA files) were obtained from UniProt https://www.uniprot.org/uniprotkb.

Research involving human participants, their data, or biological material

Policy information about studies with human participants or human data. See also policy information about sex, gender (identity/presentation), and sexual orientation and race, ethnicity and racism.

Reporting on sex and gender	*Use the terms sex (biological attribute) and gender (shaped by social and cultural circumstances) carefully in order to avoid confusing both terms. Indicate if findings apply to only one sex or gender; describe whether sex and gender were considered in study design; whether sex and/or gender was determined based on self-reporting or assigned and methods used.* *Provide in the source data disaggregated sex and gender data, where this information has been collected, and if consent has been obtained for sharing of individual-level data; provide overall numbers in this Reporting Summary. Please state if this information has not been collected.* *Report sex- and gender-based analyses where performed, justify reasons for lack of sex- and gender-based analysis.*
Reporting on race, ethnicity, or other socially relevant groupings	*Please specify the socially constructed or socially relevant categorization variable(s) used in your manuscript and explain why they were used. Please note that such variables should not be used as proxies for other socially constructed/relevant variables (for example, race or ethnicity should not be used as a proxy for socioeconomic status).* *Provide clear definitions of the relevant terms used, how they were provided (by the participants/respondents, the researchers, or third parties), and the method(s) used to classify people into the different categories (e.g. self-report, census or administrative data, social media data, etc.)* *Please provide details about how you controlled for confounding variables in your analyses.*
Population characteristics	*Describe the covariate-relevant population characteristics of the human research participants (e.g. age, genotypic information, past and current diagnosis and treatment categories). If you filled out the behavioural & social sciences study design questions and have nothing to add here, write "See above."*
Recruitment	*Describe how participants were recruited. Outline any potential self-selection bias or other biases that may be present and how these are likely to impact results.*
Ethics oversight	*Identify the organization(s) that approved the study protocol.*

Note that full information on the approval of the study protocol must also be provided in the manuscript.

Field-specific reporting

Please select the one below that is the best fit for your research. If you are not sure, read the appropriate sections before making your selection.

☒ Life sciences ☐ Behavioural & social sciences ☐ Ecological, evolutionary & environmental sciences

For a reference copy of the document with all sections, see nature.com/documents/nr-reporting-summary-flat.pdf

Life sciences study design

All studies must disclose on these points even when the disclosure is negative.

Sample size	Twenty extant laboratory mouse bones representing two different strains, six 1.7-1.8 and 1.3 myr Olduvai Gorge fossils, one 2.4 myr Chiwondo Beds fossil, one 3.0 myr Makapansgat fossil, six species-matched extant faunal bones, and eight paleosols were subject to destructive analysis. Sample data is unique to individuals.
Data exclusions	No data were excluded
Replication	Mass spectrometry data in metabolomics and proteomics is consistent within a run. All samples were run together for each omics study. Sample volumes were consumed for each specimen and run to maximize metabolite and protein recovery.
Randomization	Specimens were pre selected by curators based on criteria independent of our metabolomics research.
Blinding	All specimens were given a code, and no investigator involved in the metabolomics, the proteomics, nor the imaging had information idetifying what fossil any data was from.

Reporting for specific materials, systems and methods

We require information from authors about some types of materials, experimental systems and methods used in many studies. Here, indicate whether each material, system or method listed is relevant to your study. If you are not sure if a list item applies to your research, read the appropriate section before selecting a response.

Materials & experimental systems

n/a	Involved in the study
☒	☐ Antibodies
☒	☐ Eukaryotic cell lines
☐	☒ Palaeontology and archaeology
☒	☐ Animals and other organisms
☒	☐ Clinical data
☒	☐ Dual use research of concern
☒	☐ Plants

Methods

n/a	Involved in the study
☒	☐ ChIP-seq
☒	☐ Flow cytometry
☒	☐ MRI-based neuroimaging

Palaeontology and Archaeology

Specimen provenance: OLDUVAI GORGE RODENTS: Rene Lavocat, 1909-2007, is a french paleontologist, having worked under the direction of Camille Arambourg at the Museum National d'Histoire Naturelle de Paris to study rodents from Kenya. Having gained fame as a paleontologist of small mammals, Louis S.B. Leakey gave the fossil rodents to Dr. Lavocat in the 1960's, now curated in collections of the Institut des sciences de l evolution universite Montpellier 2, which Dr. Lavocat joined. Specimens were given to Dr. Christiane Denys in the 1980s for study, and the residuals of those studies remained with Dr. Denys until the performance of our metabolomics research. OLDUVAI GORGE SUID: L.S.B. Leakey gave this specimen to GHR von Koenigswald in 1954, it becoming a curated specimen of the Senckenberg Research Institute, Frankfurt, Germany. CHIWONDO BEDS: The elephant fossil was collected by Timothy G. Bromage and Friedemann Schrenk, it becoming a curated specimen of the Department of Antiquities, Malawi. MAKAPANSGAT: The breccia containing a fossil fragment was collected by Timothy G. Bromage and Friedemann Schrenk, it becoming a curated specimen of New York University.

Specimen deposition: The specimens were processed in destructive analyses that are no longer available.

Dating methods: n/a

☐ Tick this box to confirm that the raw and calibrated dates are available in the paper or in Supplementary Information.

Ethics oversight: No ethical approval or guidance is required for this research.

Note that full information on the approval of the study protocol must also be provided in the manuscript.

Plants

Seed stocks: *Report on the source of all seed stocks or other plant material used. If applicable, state the seed stock centre and catalogue number. If plant specimens were collected from the field, describe the collection location, date and sampling procedures.*

Novel plant genotypes: *Describe the methods by which all novel plant genotypes were produced. This includes those generated by transgenic approaches, gene editing, chemical/radiation-based mutagenesis and hybridization. For transgenic lines, describe the transformation method, the number of independent lines analyzed and the generation upon which experiments were performed. For gene-edited lines, describe the editor used, the endogenous sequence targeted for editing, the targeting guide RNA sequence (if applicable) and how the editor was applied.*

Authentication: *Describe any authentication procedures for each seed stock used or novel genotype generated. Describe any experiments used to assess the effect of a mutation and, where applicable, how potential secondary effects (e.g. second site T-DNA insertions, mosiacism, off-target gene editing) were examined.*